SEMMELWEIS EGYETEM

DOKTORI ISKOLA

Ph.D. értekezések

2848.

MAROS MÁTÉ ELŐD

Onkológia
című program

Programvezető: Dr. Bödör Csaba, egyetemi tanár

Témavezető: Dr. Krenács Tibor, kutató professzor

THE ROLE OF CELL CYCLE REGULATION IN THE PROGRESSION OF GIANT CELL TUMOR OF BONE

PhD thesis

Máté Előd Maros

Doctoral School of Pathological Sciences

Semmelweis University

Supervisor: Tibor Krenács, Ph.D., D.Sc.

Official reviewers: Gábor Lotz, MD, Ph.D.
Levente Kuthi MD, Ph.D.

Head of the Complex Examination Committee: Miklós Sárdy, MD, Ph.D.

Members of the Complex Examination Committee: Katalin Borka, MD, Ph.D.
András Vörös, MD, Ph.D.

Budapest

2023

Table of Contents

List of Abbreviations

AIC	Akaike Information Criterion
AURKA	aurora kinase A also known as serine/threonine-protein kinase 6
CD11c	integrin alpha X chain protein
CD163	cluster of differentiation 163 or high affinity scavenger receptor
CDK	cyclin-dependent serine-threonine kinases
CDKI	cyclin-dependent kinase inhibitors
CDT1	chromatin licensing and DNA replication factor 1
Cx43	gap junction connexin43
DAB	diaminobenzidine
EGFR	epidermal growth factor receptor
GCs	giant cells
GCTB	giant cell tumor of bone
H3-3A	formerly *H3F3A*, H3 histone family member 3A gene
H&E	hematoxylin-eosin staining
IFNγ	interferon-gamma
IHC	immunohistochemistry
IL-6	interleukin 6
M-CSF	macrophage colony-stimulating factor
MCM2-7	minichromosome maintenance 2-7 complex
NFκB	nuclear factor kappa-light-chain-enhancer of activated B cells
pHH3	phospho-histone-H3
PFS	progression-free survival
PP2A	Ser/Thr protein phosphatase 2A
RANKL	receptor activator of nuclear factor kappa-B ligand
PWP	Prentice-Williams-Peterson gap time survival models
Rb, RB1	retinoblastoma protein; RB1 also known as p105-RB
ROI	region of interest
SMA	smooth muscle actin
TBS	Tris-buffered saline
TMA	tissue microarrays
TNF	tumor necrosis factor

1. Introduction

1.1 Giant cell tumor of bone

Giant cell tumor of bone (GCTB) is categorized into the subgroup of osteoclastic giant cell-rich tumors besides aneurysmal bone cyst and non-ossifying fibroma according to the, current, 5th Edition of the WHO classification of soft tissue and bone tumors (1). GCTB is a locally aggressive lesion that causes pathological osteolysis predominantly affecting the epi-metaphyseal bone regions in young adults (1). It represents 2-9% of primary and ~20% of benign bone tumors (2, 3). Despite appropriate treatment, GCTB may frequently show local recurrence in 20-50% of the cases, rarely (in 1-4%) it spreads as "metastatic" emboli to the lung or it might even (in 1-10%) undergo malignant transformation (e.g. into osteosarcoma) (4-13). Histologically (**Figure 1**) GCTB is characterized by osteoclast-type giant cells that are admixed with mononuclear cells including the osteoclast precursor of monocytic/macrophage lineage and stromal cells of osteoblastic origin (3, 4). Over the years, several prognostic biomarkers including chromosomal instability, cell growth signaling and tumor microenvironment have been identified, however, none of these became integrated into the daily diagnostic praxis (6, 14-18). Hence, predicting the clinical progression of GCTB from histopathological features remains a diagnostic challenge.

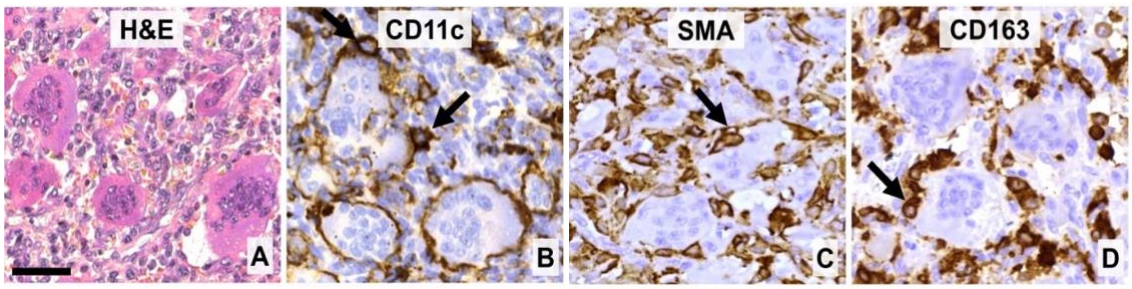

Figure 1. The main cell components of giant cell tumor of bone. (A) Multinucleated giant cells (GCs) are admixed with mononuclear and red blood cells (hematoxylin-eosin staining, H&E). (B) GCs and their monocytic precursors carry the CD11c marker while (C) Neoplastic stromal cells are characterized by smooth muscle actin (SMA) positivity. (D) Histiocytes and monocytic GC precursors but not GCs express the CD163 scavenger receptor. Arrows emphasize positive cells in proximity of GCs potentially capturing fusion. Diaminobenzidine (DAB, brown) immunoperoxidase reactions (B-D). Scale bar: 50 µm for all images. Modified from (19) and used with permission of the publisher under the terms of the Creative Commons Attribution License (CC BY).

1.1.1 Mononuclear cell fraction

The mononuclear cell fraction of GCTB (**Figure 2**) consists of osteoclast precursors of monocytic/macrophage lineage and spindle-like stromal cells of osteoblastic origin (4, 20). The stromal cells are thought to be the neoplastic cell fraction that drive the abnormal osteoclastogenesis in GCTB (21-23).

Accordingly, stromal cells have demonstrated chromosomal instability (24), telomeric associations (25, 26) and elevated proliferative activity (18). Hallmark mutations in the H3 Histone Family Member 3A (*H3-3A*, formerly *H3F3A*) gene were identified in >90% of GCTB cases, dominantly at Gly34 (17, 27-30). Stromal cells regulate osteoclastogenesis through cytokine secretion including macrophage colony-stimulating factor (M-CSF), interferon-gamma (IFNγ), and the growth factor from the tumor necrosis factor (TNF) family, called receptor activator of nuclear factor kappa-B (NFκB) ligand (RANKL) (20, 21, 31). The overexpression of M-CSF and RANKL are the main drivers of osteoclast and giant cell formation and lytic activity. Our research group has shown elevated epidermal growth factor receptor (EGFR) expression (6) and reduced and deregulated intercellular connections, mainly reduced gap junctions of connexin43 (Cx43) channels in the neoplastic stromal cell fraction of recurrent and malignant GCTB cases (15). Concurrent changes of the extracellular matrix (**Figure 2**) further facilitate cell mobility, blood monocyte invasion and macrophage polarization, mainly by the overexpression of tenascin and underexpression of decorin and lumican (23).

Since GCTB can lead to substantially reduced quality of life or even death, it is crucial to identify patients with increased risk of recurrence. Therefore, in this study, we aimed to correlate (**2. Objectives: 1.**) the proliferating mononuclear cell fractions with progression-free survival (PFS) using their DNA index (ploidy) and tissue microarrays using immunohistochemistry through detecting nuclear cell cycle regulation-linked proteins mentioned below (**1.2 Cell cycle regulation**) in osteoclast rich regions of GCTB.

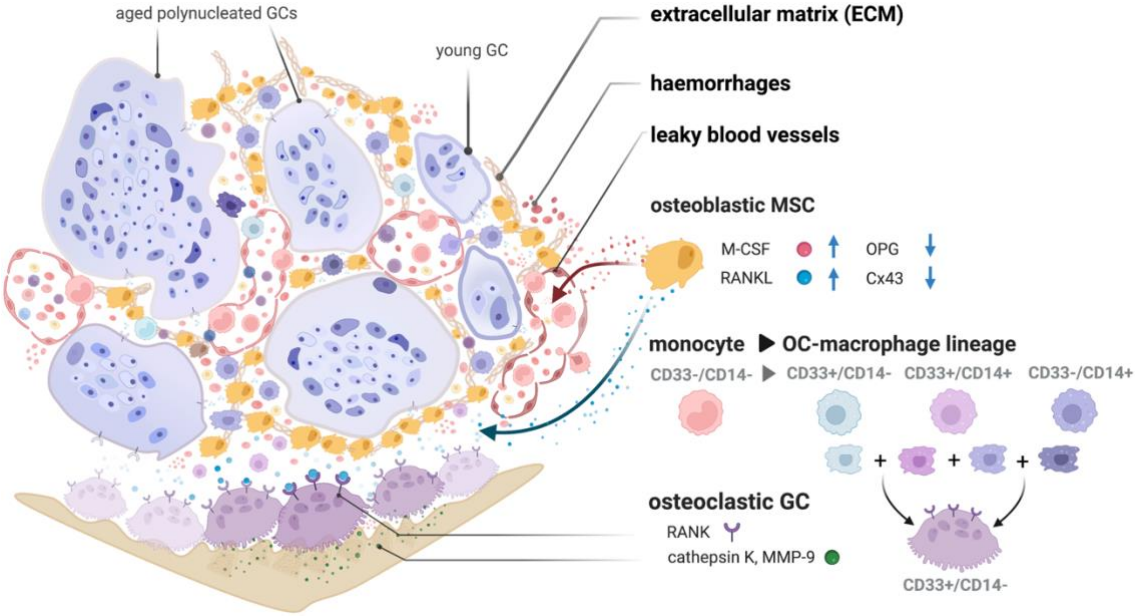

Figure 2. Overview of main cellular components of GCTB and the giant cell fusion process. The main neoplastic drivers are the osteoblastic mononuclear spindle-shaped cells (MSC; yellow), which harbor the hallmark *H3-3A* (formerly *H3F3A*) gene mutation, telomeric associations and genomic instability, also reduced gap junctions (Cx43) and intercellular connectivity. MSCs excessively secrete M-CSF (red arrow) and RANKL (blue arrow) while reducing the production of the RANKL-decoy receptor osteoprotegerin (OPG), consequently changing the local and vascular microenvironment and attracting CD33-/CD14- blood monocytes (light red). These monocytes then commit to the osteoclastic-macrophage transition (light turquoise, violet, blue), become tissue-specific and change their cellular surface profiles. GCs are then formed by the fusion ("+") between pre-osteoclasts and osteoclastic macrophages with CD33+/CD14-, CD33+/CD14+ or CD33-/CD14+ surface antigens. Finally, osteoclastic GCs express RANK and CD33+ while being negative for CD14 and CD163. To note that all GCs are located in the immediate vicinity of and are associated with leaky blood vessels indicating their monocytic origin. Due to the (osteo)lytic activity of GCs (primarily by effector enzymes like cathepsin K and MMP-9), hemorrhages occur frequently and are linked to more aggressive phenotypes. Concurrent changes of the extracellular matrix (ECM) support cell mobility by overexpressing tenascin C and under expressing decorin and lumican. Abbreviations: GC, giant cells; OC, osteoclastic; M-CSF, macrophage colony-stimulating factor; RANK, receptor activator of nuclear factor kappa-B and its ligand (RANKL); Cx43, connexin 43; MMP-9, matrix metalloproteinase-9. The figure was modeled after **Figure 1B** and created with BioRender.com.

1.1.2 Multinucleated giant cells

Multinucleated giant cells (GC) can form two distinct ways: i) through acytokinetic cell division and ii) by cell fusion. The former is the result of incomplete cell division due to cytoskeletal malfunctions (32, 33), which is typical of proliferating neoplastic cells, such as Reed-Sternberg cells in classical Hodgkin lymphoma (34) or multinucleated tumor cells in soft tissue myxofibro- and osteosarcomas (7, 28). While osteoclast-type giant cells of GCTB are formed by fusion of cells of the monocyte-macrophage lineage (35), similar to inflammatory multinucleated GCs (36), such as Langhans-type GCs and foreign body GCs (37).

In GCTB (**Figure 2**), the tumor microenvironment attracts (primarily through M-CSF and RANKL) myeloid progenitor cells and monocytes to extravasate from the blood into the tumor and initiate their transition to macrophages (23, 38). At first, these (non-osteoclastic) macrophages bear a CD14- and CD33- double-negative cell surface marker profile (23, 39). Through the upregulation of M-CSF and RANKL by neoplastic spindle-formed stromal cells, pre-osteoclasts and GCs, monocytes undergo the polarization process (40) and become tissue specific while committing to the macrophage-osteoclast axis (38, 41). Besides RANK, osteoclast-committed macrophages can express CD14+ and/or CD33+ on their cell membranes (23). Pre-osteoclasts and osteoclastic GCs retain RANK and CD33+ but do not express CD14 (**Figure 2**) or CD163 (**Figure 1D**). Ultimately, GCs and large osteoclasts are created by fusion of pre-osteoclasts and osteoclast-committed macrophages (16, 23).

GCs are the effectors responsible for pathological bone resorption in GCTB (**Figure 2**), hence, they require continuous stimuli from neoplastic stromal cells to be able to fuse from pre-osteoclasts and to progressively resorb bone (42, 43). These proliferative factors include the above mentioned canonical pathway (M-CSF/RANK/RANKL) and various other (non-canonical) growth factors (16) such as vascular endothelial- (VEGF) hepatocyte- and placental growth factors as well as hypoxia inducible factors 1α and 2α (43, 44). Also, TNF-α can promote monocyte/macrophage fusion and osteoclastogenesis, similar to acute inflammation through interleukin 1 beta (IL-1β) (42). Whereas other members of the interleukin family (IL-3, IL-4, IL-6) are more important for inflammatory and foreign body-type GC formation (16, 44).

Despite this reactive, osteoclastic origin of GCs (45), their nuclei show diverse proportions of immunoreactions for general proliferation (Ki67) and G1-phase cell cycle markers such as cyclin D1-D3 and inhibitors like $p21^{WAF1}$ and $p16^{INK4a}$ (18, 37, 46-48). However, a comprehensive approach including cell cycle control proteins of licensing and late-phase (S-G2-M) promoters had not been investigated before (**Figure 3**).
Therefore, we scrutinized the expression of cell cycle regulatory proteins using a comprehensive set of markers to see if GCs in GCTB show replicative activity and if it is of clinicopathological relevance (**2. Objectives: 2.**).

1.2 Cell cycle regulation

Cell division is comprised of two major phases, the process of nuclear and cellular division called mitosis (M-phase) and the interphase between two mitoses (49-51). The interphase can be subdivided further into the G1 ("gap") phase that precedes DNA replication, the S-phase when new DNA is synthesized and the second gap (G2) phase preceding mitosis (**Figure 3**). Under unfavorable conditions, such as high cellular density or absence of growth factors, cells can exit the cell cycle from G1 and temporarily enter the resting state of quiescence (G0-phase), which is reversible once the conditions become pro-proliferative again. In case of severe DNA damage or aging, however, cell cycle arrest can occur at G1-, G1/S- or G2-phases and induce the irreversible state of senescence, which is also required for cellular homeostasis such as functional maturation, hypertrophy and secretory activities (52-54). The summary of investigated cell cycle-regulatory markers is presented in **Table 1**.

Cells have a sensitive window at the early G1-phase (55) called the restriction point to overcome (**Figure 3**) to access the cell cycle (56). This process is called licensing that involves the heterohexameric ring complex of minichromosome maintenance 2-7 (MCM2-7) proteins (57, 58). Besides the general proliferation marker Ki67, MCM2-7 complex proteins can also be detected throughout the cycle except in quiescence (G0) (52). Thus, they can be used as markers of growth fractions in tumors (50, 51, 59). Next, complexes of cyclins and cyclin-dependent serine-threonine kinases (CDK) drive the cells through major phases of the cycle (60).

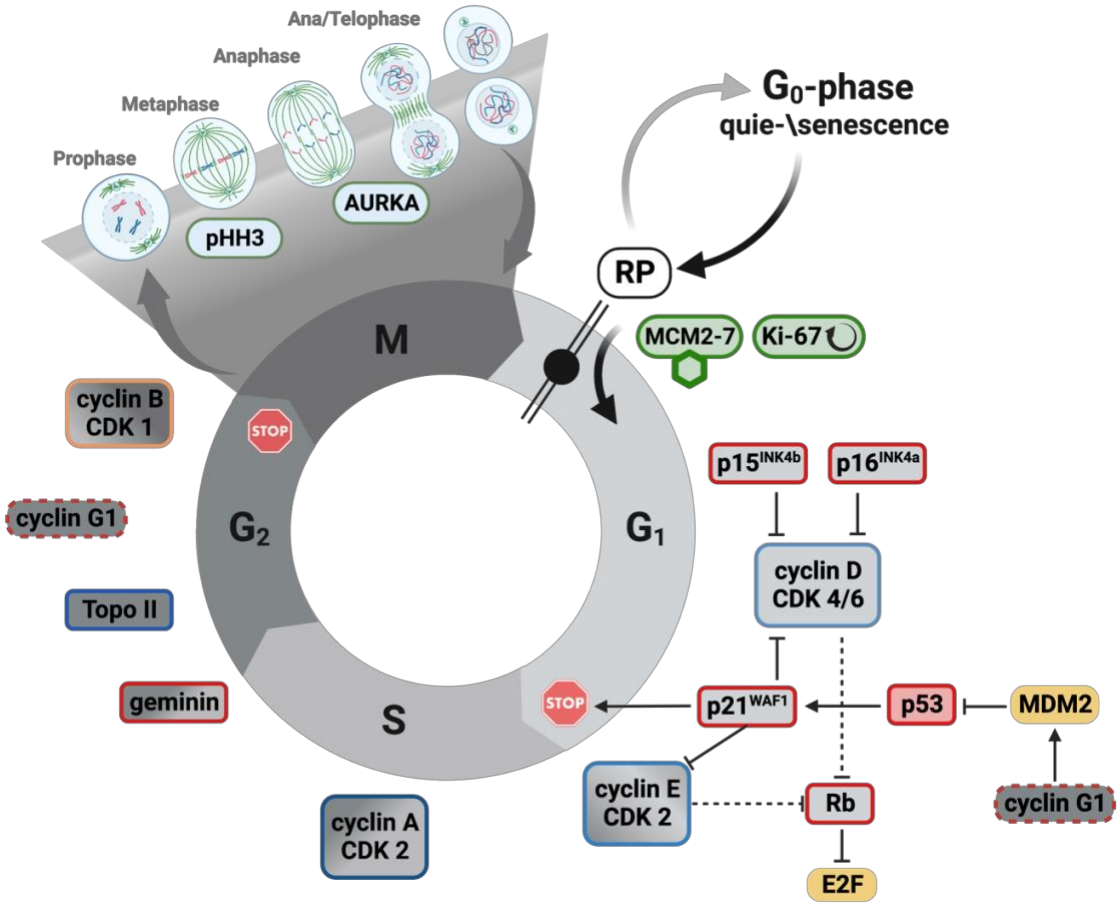

Figure 3. Overview of the cell cycle machinery and the investigated regulatory proteins. Arrows indicate activating- while "T" signs represent inhibitory functions. Stop signs signal the G1/S and G2/M checkpoints. RP (double line with dot) marks the restriction point. General proliferation marker (Ki67) and the hexamer licensing complex (MCM2-7) are shown in green, both of which can be detected during the whole cell cycle (circular arrow). Gray background color gradients indicate protein activity matched to respective phases of the cell cycle. Cyclin-CDK complexes, framed with shades of blue, support the respective G1-S-G2-M transition, according to their positions. Inhibitory markers of the INK4 ($p15^{INK4b}$, $p16^{INK4a}$) and CIP/KIP families ($p21^{WAF1}$), the genomic guardian (p53) and repressor (geminin) are framed in red. Cyclin G1 with dashed red frame is depicted twice to indicate its dual pro- and antiproliferative roles. Markers with yellow frames (cyclin B-CDK1) or backgrounds (MDM2, E2F) were not evaluated systematically in our projects. Phases of mitosis (M) are magnified as an inset. Phosphohistone H3 (pHH3) and the "polar kinase" (aurora kinase A, AURKA) are positioned below the phases of their strongest activity at the meta- and ana-/telophases, respectively. The image was in part modeled after figures published in (19) and was created with BioRender.com.

According to the classic view, G1-S-phase transition is primarily initiated by D-type cyclins (61). Cyclin D1-CDK4/6 are the key drivers of G1/S-phase transition by phosphorylating retinoblastoma (Rb) protein (RB1) and other "pocket" proteins p130 and p107 (also called Rb-like protein 1 and -2, respectively) (62-65). Thus, the inhibitory control of transcription factor E2F is reduced, which promotes the transcription of cyclinE-CDK2, resulting in a positive feedback loop (51). This can be prevented by cyclin dependent kinase inhibitors (CDKI) specifically targeting CDK4/6 like $p15^{INK4b}$, $p16^{INK4a}$ and by general inhibitors from the CIP/KIP family as $p21^{WAF1}$ and $p27^{KIP1}$ targeting both cyclin D1 and cyclin E-CDK complexes (60, 66-68). During S-phase, the cyclin A-CDK2 complex mediates transcriptional control of DNA synthesis and drives S/G2-phase transition (66, 69), whilst topoisomerase 2a mediates post-G1-phase DNA cleavage and reassembly (70, 71).

In late G2-phase, cyclin A also binds to CDK1 and promotes G2/M-phase transition (51, 72). Concurrently, the DNA replication repressor geminin prevents the repeated replication licensing in post-G1-phase through binding to CDT1 (chromatin licensing and DNA replication factor 1); hence, blocking the re-loading of the MCM2-7 complex onto chromatin (49, 52, 73-75). Finally, the cyclin B1-CDK1 complex catalyzes mitotic cell division (47, 69, 76) by activating the microtubule assembly, chromatin and DNA relaxation for increased gene transcription through the phosphorylation of H1 and H3 histones (pHH3) (77). Concurrently, the G2- and M-phase-related aurora kinase A (AURKA), the "polar kinase", facilitates the mitotic division by stabilizing the centrosome through associating with the mitotic poles and adjacent spindle microtubules (59, 62, 71, 78).

Checkpoint failures during mitosis (M-phase) can cause chromosomal instability and incorrect cytokinesis with alterations during sister-chromatid separation resulting in poly- or aneuploidy (79), which can contribute to tumor development (66, 79). Ploidy can be reliably detected by DNA content measurement using flow-cytometry (18, 80, 81) and quantified by the DNA index that is the ratio of G0/G1 peaks in cell populations compared to normal bone marrow (82).

The tumor suppressor p53 plays a crucial role in preventing aneuploidy through G1 cell cycle arrest by either activating DNA damage response genes or inducing programmed cell death, if the defective DNA cannot be repaired (83). As a p53 target, cyclin G1 has

dual functions as it can facilitate both cell cycle arrest and S-G2-M progression (84). For the latter, cyclin G1 might activate the MDM2 oncoprotein by recruiting Ser/Thr protein phosphatase 2A (PP2A), which dephosphorylates MDM2 to inhibit and degrade p53 (84-87). The p53-dependent G1 arrest of multinucleated tetraploid cells has been previously described (83) and p53 activity with the contribution of $p21^{WAF1}$ can also drive this process even further to result in cellular senescence (33).

Table 1. Occurrence of cell cycle-regulation markers during the replication cycle and the applied antibodies for their detection**.**

Antibody	Clone	Vendor	Dilution	Locali-zation	Activity in cell cycle phases			
					G1	S	G2	M
Ki-67	MIB-1	Dako	RTU	N	+	++	++	++
Ki-67	SP6	Th-LV	1:600	N	+	++	++	++
Ki-67	B56	HisPat	RTU	N	+	++	++	++
MCM2	CRCT2.1	Th-LV	1:200	N	++	++	++	++
MCM6	PA5-79649	Th-LV	1:600	N	++	++	++	++
cyclin D1	SP4	Th-LV	1:200	N	+	++	+	+
cyclin E	13A3	Th-LV	1:20	N	++	++	-	-
CDK4	DCS31+35	Th-LV	1:300	N/CP	+	+	-	-
CDK2	2B6	Th-LV	1:300	N/CP	+	++	+	-
cyclin A	6E6	Th-LV	1:500	N	-	++	+	+
cyclin G	11C8	Th-LV	1:00	N				
geminin	EM6	L-NC	1:150	N	-	++	+	+
p-HistH3.3 (Ser10)	K.872.3	Th-Inv	1:100	N	-	-	-+	++
$p15^{INK4b}$	15P06	Th-LV	1:200	N/CP	+			
$p16^{INK4a}$	JC8	Th-LV	1:200	N/CP	+			
$p21^{WAF1}$	SX118	Dako	1:150	N	+	++	+	-
p53	DO7	Th-LV	1:100	N	+	+	+	+
retinoblastoma	1F8	Th-LV	1:100	N	++	+	-	-
Topoisomerase 2a	Ki-S1	Th-LV	1:200	N	-	+	++	++
aurora kinase A	1G4	CS	1:80	CP	+	+	++	++

CP: cytoplasmic; N: nuclear; -: negative; +: moderate; ++high; Antibody vendors: Dako (Glostrup, Denmark); Th-LV: Thermo Fisher-Labvision (Fremount, CA USA); Th-Inv: Thermo Fisher-Invitrogen; L-NC: Leica-NovoCastra (Newcastle upon Tyne, UK); HisPat: Histopathology (Pecs, Hungary). RTU: ready-to-use; CS: Cell Signalling (Danvers, MA, USA);

These proteins regulating cell replication can be reliably detected (69) *in situ* using immunohistochemistry for the assessment of cell cycle fractions in archived tissues (50). As cell cycle is a downstream integrator of pro- and antiproliferative signaling pathways, accelerated cell cycle progression has been associated with genomic instability, elevated tumor grade and aggressiveness resulting in reduced disease progression-free survival (PFS) in various tumors including breast- (73), colorectal- (88) and lung adenocarcinomas (89), as well as in melanomas (71), and in Ewing's sarcoma family of tumors (90).

Similarly, elevated cell proliferation has already been linked to GCTB progression, however, so far only small patient cohorts have been tested using either only general proliferation markers or those expressed only at early phases of the cycle (18, 46-48). On the other hand, recurrence potential in a larger cohort was controversially linked to p53 and cyclin D1 upregulation in mononuclear and GCs, respectively (91). The association between mononuclear cell cycle fractions and PFS in GCTB has not yet been properly investigated.

2. Objectives

Since elevated cell replication is often associated with aggressive tumor behavior and poor disease prognosis (51), the doctoral thesis project had two main objectives:

1. To study if cell cycle fractions in the mononuclear cell compartment can help predict the clinical prognosis of GCTB using progression-free survival – investigated in Maros et al, 2019 (92).

   In detail, the first objective of this research project was to characterize the proliferating mononuclear cell fractions through detecting nuclear cell cycle regulation-linked proteins in osteoclast rich regions of tissue microarrays using immunohistochemistry. The comprehensive marker profile included the general cell cycle marker Ki67 replication licensing (MCM2), G1-phase (cyclin D1, CDK4), post-G1-phase (cyclin A and CDK2) and M-phase (phospho-histone-H3) markers, the cyclin dependent kinase inhibitor $p21^{WAF1}$ and the replication repressor geminin proteins. Additionally, the flow cytometry-based DNA index (ploidy) was also analyzed.

2. To investigate whether cell cycle regulation can be linked to GC formation and activity, thereby predicting local osteodestruction (grade) and phenotype of GCTB cases – investigated in Maros et al, 2021 (19).

   In detail, cell cycle activity in GCs was profiled to see if it is different between primary and recurrent GCTBs. We tested the expression of cell cycle regulatory proteins in GC nuclei including 3 clones of the general proliferation marker Ki67; the DNA replication licensing factors (MCM2 and MCM6); the G1-S-phase markers (cyclin D1 and its complexing partner CDK4/6); the early (CDK2 and cyclin A) and late (topoisomerase 2a) post-G1-phase markers; and additional G2-M-phase markers (AURKA and pHH3). Furthermore, the DNA replication inhibitor geminin and CDK-inhibitors $p15^{INK4b}$, $p16^{INK4a}$, $p21^{WAF1}$ and $p27^{KIP1}$ as well as the oncosuppressor retinoblastoma and p53 and its target the unpaired cyclin G1 were also examined.

3. Methods

3.1. Study cohort

We performed single-center retrospective cohort studies within the EuroBonet network using 154 distinct formalin-fixed and paraffin-embedded surgical cases from 139 GCTB patients, who were diagnosed and operated between 1994-2005 at Institute of Rizzoli, Bologna (IOR), Italy. The studies were approved by the ethical review boards for human research at both the Semmelweis University, Budapest, Hungary (approval nr.: 87/2007) and at the IOR (approval nr.: 13351/5-28-2008) and were performed in accordance with the Declaration of Helsinki. All adult patients or both parents of minors have provided a written informed consent (92).

The study focusing on the mononuclear cell fraction included all 154 surgical cases of 100 primary (P), 37 first- (1-Rec), 16 second-/or higher recurrences (2-Rec/3-Rec) GCTBs and one metastasis) (92). For the systematic analysis of GCs, a stratified random sample of 10-10 P and 1-Rec distinct cases was generated from the above cohort (19).

3.2. Tissue microarray (TMA)

Tissue microarrays (TMA) blocks (**Figure 4**) were created from the archived 154 surgical tissue samples using a 10 x 7 grid pattern of 2 mm diameter tissue cores (92). Altogether, four TMA blocks were analyzed, which contained 215 TMA tissue cores including duplicates from 56 surgical cases (n_{cores}=112), triplicate from a single case (n_{cores}=3) and a single core from each of the remaining 100 surgical cases. Of these, 4 μm thick sections were cut and brought onto dewaxed slides.

3.3. Immunohistochemistry (IHC)

Immunostainings of cell cycle proteins were performed on sections cut from TMA blocks. The primary antibodies (**Table 1**) were either mouse or rabbit monoclonal primary antibody clones, or rabbit polyclonal immunoglobulins (**Figure 4**), which were incubated overnight (~16h) at room temperature including anti-Ki67 Mib1, -B56, -SP6, -MCM2, -MCM6, -CDK2, -CDK4, -cyclin D1, -cyclin E, -cyclin G, -cyclin A, topoisomerase 2, -aurora kinase A, -pHH3Ser10, -p53, -retinoblastoma, -$p15^{INK4b}$, -$p16^{INK4a}$, -$p21^{WAF1}$ and also rabbit polyclonal immunoglobulins for -geminin, -p53 and -retinoblastoma (92). Endogenous peroxidase activity was quenched using 0.5 % hydrogen peroxide in

methanol for 20 min. Tissue-bound antibodies were detected using the NovoLink polymer peroxidase kit (Leica-NovoCastra). Both the post-primary reagents and the polymer-peroxidase complex were applied for 30 min. Between incubation steps the slides were washed for 2x3 min in 0.01 M pH 7.4 Tris-buffered saline (TBS) containing 0.1% Tween 20 (92). Peroxidase activity was revealed using a hydrogen peroxide/diaminobenzidin (DAB) substrate-chromogen kit (DAB Quatro kit, Thermo-Fisher) for 3–5 min. For eliminating previously used immunosequences and thus the unwanted cross reactions when primary antibodies of the same species were combined, a 5 min boiling of slides in TE buffer was performed between consecutive immunoreactions (19). Finally, the slides were counterstained with hematoxylin and coverslip mounted (92).

For double labelling DAB-peroxidase reactions were combined with 3-amino-9-ethylcarbazole (AEC)-peroxidase reactions (92). For double immunofluorescence (mouse Ki67 Mib1; rabbit cyclin D1 and cyclin A) antibodies, were detected simultaneously using Alexa Fluor 488 (green) goat anti-mouse IgG and Alexa Fluor 564 (red) goat anti-rabbit IgG (92).

3.4. DNA flow cytometry

DNA content measurement was performed using flow-cytometry at the IOR, Italy (93). For this, nuclear suspension of trimmed cryopreserved GCTB tissue was evaluated according to a modified method after Vindelov et al. (80, 81) using BD Cycletest Plus DNA Kit (BD Biosciences, San Jose, CA, USA). Two thousand cell nuclei per surgical case were measured using BD fluorescence-activated cell sorting (FACS) scan and analyzed in the BD CellFit™ software (93). DNA content was quantified by the DNA index (DI), which was calculated as the ratio of G0/G1 peaks of cell populations in GCTB specimens compared to the reference of normal bone marrow samples (82). Diploid and poly-/aneuploid cases were defined as DI=1 or DI≠1, respectively.

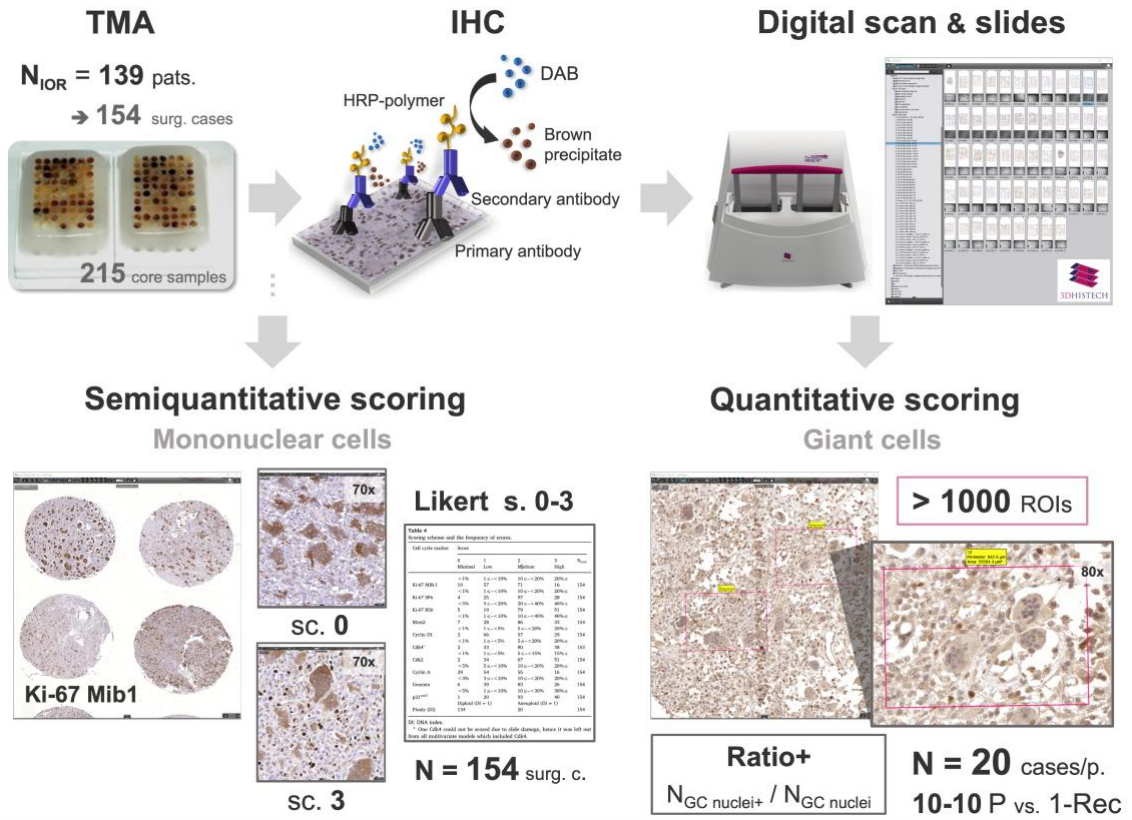

Figure 4. Overview of the applied methods and scoring schemes. The tissue microarray (TMA) core samples of 139 GCTB patients from the Institute of Rizzoli (IOR, Bologna, Italy) were immunostained (IHC) with a comprehensive set of cell cycle markers (**Table 1**) and scanned using the depicted Pannoramic Scan II System. Subsequently, the digitalized slides were then scrutinized in the CaseViewer software (3DHISTECH). The mononuclear cell fraction was evaluated using a semiquantitative scoring scheme based on four-point Likert scales in 154 surgical cases with varying, cell cycle marker-specific thresholds. The insets show 1-1 case with a score 0 (minimal) and score 3 (high) proportion of positive mononuclear cells with Ki-67 (Mib1) staining, respectively. The giant cell (GC) content was quantitatively evaluated in a stratified random subset of 10-10 primary (P) and first-recurrence (1-Rec) cases, in >1000 regions of interest (ROI, magenta rectangle) at 80x HPF. During this, the number of GCs (N_{GC}), number of GC nuclei (N_{GC_nuclei}), and respective cell cycle marker positive GC nuclei ($N_{GC\_nuclei+}$) were manually counted per ROI and averaged over all cell cycle markers for each surgical case for more robust estimates. The most practical estimator was the ratio of marker positive nuclei (ratio+ = $N_{GC\_nuclei+}/N_{GC\_nuclei}$; grey rectangle). These generated descriptive features combined with poly-/aneuploidy (DNA index) were assessed in downstream statistical analyses and modeling approaches.

3.5. Digital microscopy and image analysis

3.5.1. Mononuclear cells

The immunostained TMA sections were digitalized using a Pannoramic Scan II System (**Figure 4**) and analyzed using its CaseViewer software (both 3DHISTECH, Budapest, Hungary). For the mononuclear cell fraction (92), each cell cycle marker was manually evaluated by three independent blinded readers in three different GC rich high-power fields (HPF, 40x) of each of the 215 TMA cores. They counted the proportion (%) of the nuclear reactions in marker positive mononuclear cells in relation to all mononuclear cells. Then, a distinct cut-off threshold was set for each marker by averaging the results among readers and converting it to a four-point Likert scale (minimal 0, low 1, medium 2, high 3 proportion). In case of discrepant Likert-scores of dupli- or triplicate parallel TMA cores, the highest value was taken during statistical analyses.

3.5.2. Multinucleated giant cells

For GCs (19), the number of GCs (N_{GC}), number of GC nuclei (N_{GC_nuclei}), and respective cell cycle marker positive GC nuclei ($N_{GC\_nuclei+}$) were counted in three GC rich regions of interest (ROI) at HPF 80x per TMA core in the random subcohort of 20 surgical cases while N_{GC} and N_{GC_nuclei} were additionally averaged over all cell cycle markers for each surgical case for more robust estimates (**Figure 4**). Furthermore, the ratio for each staining ($N_{GC\_nuclei+}/N_{GC\_nuclei}$) were also calculated to allow for more stable and direct comparisons across cell cycle markers.

3.6. Statistical analyses

All statistical analyses were exploratory and performed in the R (v.3.6.3, Vienna, Austria) and SAS (v.9.4, Cary, NC, USA) statistics programs.

The primary focus of our study concerning the cell cycle activity of the mononuclear cell fraction (**4.2 Mononuclear cell fraction**) was progression-free survival (PFS) defined as follows: recurrence, local- (i.e. bone) or lung metastases (i.e. “tumor emboli”), malignant transformation (e.g. into osteosarcoma) or death of any cause, which made up a total of 40 progression events during follow-up.

To our knowledge this was the first time that the clinical progression of GCTB was evaluated by properly incorporating the increased risk of consecutive recurrence events by using Prentice-Williams-Peterson gap time models (PWP) (94). In contrast to classical

Cox proportional hazard regression, PWP models can account for multiple consecutive progression events during the follow-up of a patient by assigning increasing hazards for the next progression after subsequent events (95-97).

For this both uni- and multivariate PWP-GT models were evaluated, also testing all possible combinations up to 5 variables including cell cycle markers (assessed on a four grade Likert-scale) (98) and clinicopathological factors such as age at diagnosis, gender, localization, and treatment type using automated variable selection based on the Akaike Information Criterion (AIC). AIC is favorable in the setting of small number of events to find the optimal number of predictor variables (99). Also, all feasible interaction models were assessed to uncover possible interactions between cell cycle marker expression levels and clinical factors (100). Finally, as sensitivity analyses, all models were refitted as time-to-first-event analyses on a subset of cases (n=135) after the exclusion of four patients with incongruent staining results to evaluate if previously proposed models stayed stable (92). Additionally, Spearman's rank correlation-based unsupervised clustering was also investigated.

For GCs (**4.3. Multinucleated giant cells**), the Jonckheere–Terpstra test was used to investigate the overall difference between Enneking's/Campanacci's grading (i.e. latent, active and aggressive), GC count and GC nuclear positivity (19). As post hoc test, nonparametric Wilcoxon-Mann-Whitney U tests were applied to compare the mean rank of N_{GC}, N_{GC_nuclei}, and $N_{GC\_nuclei+}$ as well as their ratios ($N_{GC\_nuclei+}/N_{GC\_nuclei}$) between P and 1-Rec samples. Possible associations between $N_{GC\_nuclei+}$ and time-to-first-progression event were also analyzed (19). P-values were adjusted for multiple testing to counteract type 1 error inflation using the conservative Bonferroni correction. Adjusted p-values (p^*) <0.05 were considered significant.

4. Results

4.1. Study cohort characteristics

A single-center retrospective cohort study was performed on 154 formalin-fixed and paraffin-embedded GCTB samples from 139 patients, which were surgically removed and diagnosed between 1994-2005 at Institute of Rizzoli, Bologna (IOR), Italy (92).

The study (92) focusing (**2. Objectives: 1.**) on the mononuclear cell fraction included 154 surgical cases comprised of 100 primary (P), 37 first- (1-Rec), 16 second-/or higher recurrences (2-Rec/3-Rec) and one metastasis. Each sample from the same patient taken at different time points during the course of the disease (i.e. primary, its recurrence or consecutive recurrences) was considered as a separate diagnostic case. Thereby, 16 patients had 33 consecutive cases. A total of 40 progression events occurred during the median follow-up of 85 months (range: 1-340 months/28,3years). Three quarter of the cases (74%; 114/154) had benign course, while progression events occurred in 26% (40/154) of which local recurrences were 62.5% (25/40) and 15% (6/40) showed malignant transformation to osteosarcoma with fatal outcome (92). Pulmonary "metastases" (emboli) were found in 13 cases (8.4%) during the entire disease course. The overall mortality rate was 7.9% (11/139). Surgical staging (1-3) by Enneking (101) or radiological grade by Campanacci et al. (102), both equivalent with the clinical latent (L: 42/139, 30.2%), active (A: 40/139, 28.8%) and aggressive (Ag: 57/139, 41.0%) stages were available for all patients (92).

As first treatment 74 (53.2%) patients underwent curettage with local adjuvants (primarily phenol, 65/74), fifty (36%) tumors were resected (with wide margin 42/50), three excised and one amputated, while 11 (7.9%) patients received additional radiotherapy.

The study (19) investigating cell cycle activity in GCs (**2. Objectives: 2.**) was performed on a stratified random sample of 10 primary tumors (P) and 10 first recurrences (1-Rec) surgical cases from the above cohort of 139 patients (19). In these 20 patients, 12 progression events were registered (60%) during follow-up. Eight-eight patients (40%) were continuously disease free or had local recurrences respectively, 2 (10%) were alive with disease at last follow-up while malignant transformation (osteosarcoma) and stroke both with consecutive fatal outcomes occurred in 1-1 patients (5%), respectively.

4.2 Mononuclear cell fraction

4.2.1 Cell cycle marker detection in GCTB mononuclear cells

All cell cycle markers showed nuclear immunoreaction (except CDK2 and CDK 4, which showed some additional cytoplasmic staining). Positive cells were predominantly found in the mononuclear cell fraction of GCTB, except for cyclin D1 and $p21^{WAF1}$, which were also detected in GCs. To note, however, that only mononuclear cells were considered at scoring. While most proliferating (Ki67 positive) mononuclear cells were CD163 negative, many of them were α-SMA positive indicating a stromal origin (**Figure 5**).

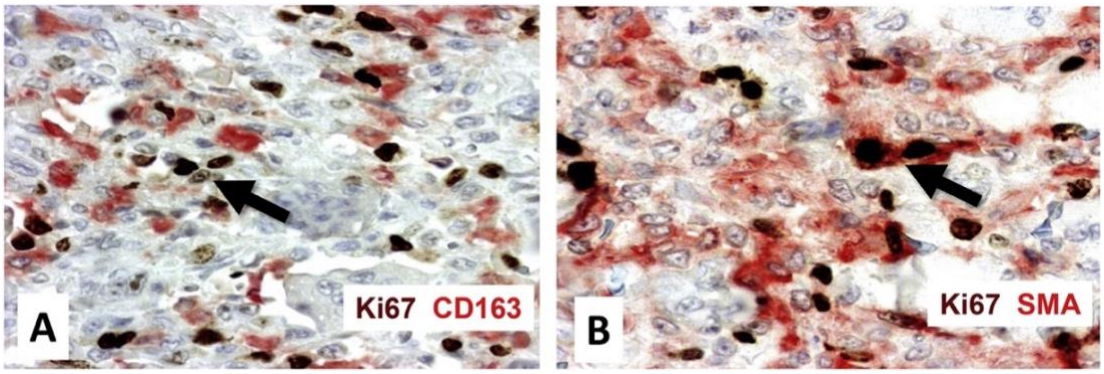

Figure 5. The majority of the proliferating, Ki67 positive mononuclear cells were CD163 negative (A, arrow), while many of them show smooth muscle actin (SMA) positivity (B, arrow) indicating their osteoblastic stromal origin. The image is used with the permission of the publisher (92) under the terms of the Creative Commons Attribution License (CC BY).

4.2.2 Correlation-based hierarchical clustering of cell cycle marker expression

Hierarchical cluster analysis, based on Spearman's rank correlations of the visual four-point Likert scale scoring of these markers, showed no major defect of the cell cycle regulation in GCTB (**Figure 6**). CDKs showed the highest correlation with their respective complexing cyclins (CDK2-cyclin A, r_{SP}=0.56) or inhibitors (cyclin D1-$p21^{WAF1}$, r_{SP} =0.51) and clustered around each other, except for CDK4. Also, the general proliferation marker Ki67, the replication licensing factor MCM2 and its repressor geminin formed a common subcluster with the highest associations (r_{SP} =0.59-0.68). This again supported the notion that cell cycle regulation is not seriously deregulated in mononuclear cells of GCTB.

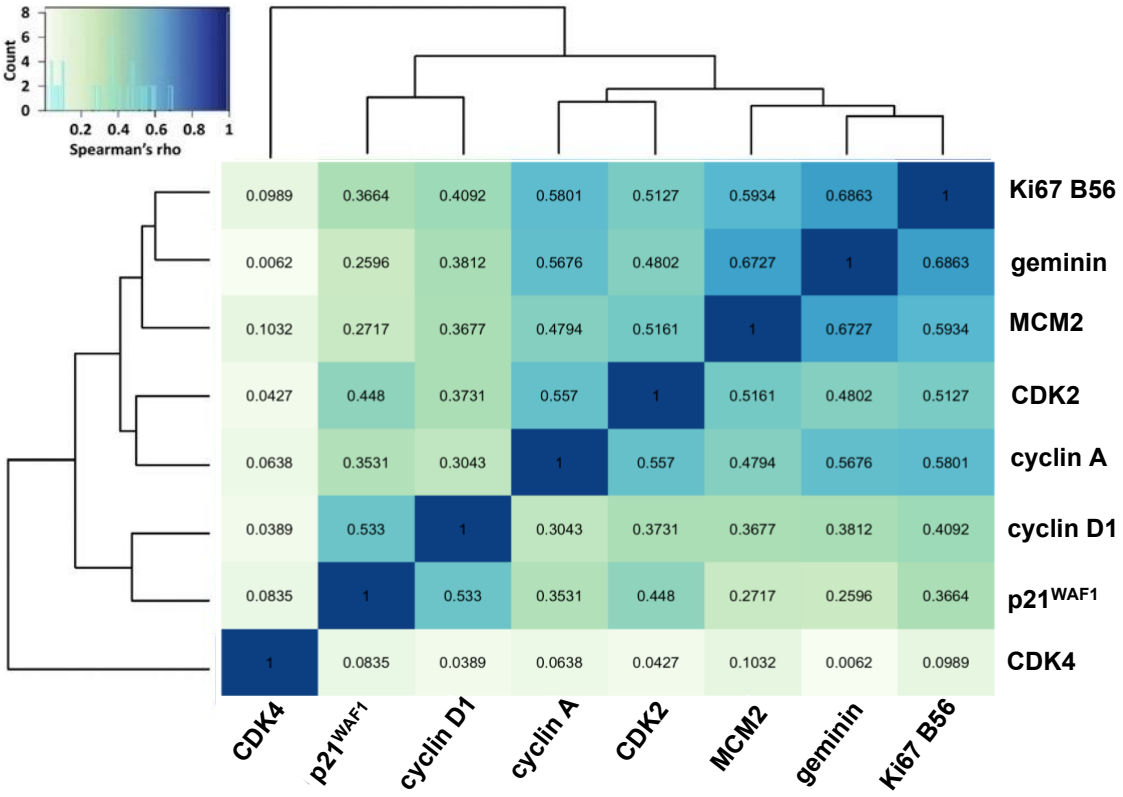

Figure 6. Heatmap and dendrograms of unsupervised hierarchical clustering of cell cycle marker expression in GCTB mononuclear cells. Numbers inside the boxes represent the Spearman's rank correlation coefficients (r_{SP}) of the 4-grade visual scoring and in the color scheme (upper-left corner). Licensing-related enzymes (Ki67, MCM2-geminin), CDKs and their respective cyclins (CDK2-cyclin A) or inhibitors (cyclin D1-$p21^{waf1}$) were clustered closest to each other in line with their regulatory functions in a "normal" replication cycle. Figure used from (92) with permission of the publisher under CC BY license.

4.2.3 Univariate progression-free survival analyses

Univariate survival analysis using PWP gap time models (**Figure 7**) revealed that poly-/aneuploidy (HR=5.33, 95%CI: 3.52-8.07, p<0.0001) against diploid chromosome set and elevated cyclin A (HR=2.84, 95%CI: 2.07-3.89, p<0.001), geminin (HR=2.48, 95%CI: 1.70-3.61, p=0.015), MCM2 (HR=3.44, 95%CI: 2.06-5.73, p=0.016) and cyclin D1 (HR=2.20, 95%CI: 1.56-3.10, p=0.022) positive mononuclear cell fractions had significant negative association with PFS. Of the Ki67 immunoreactions, B56 (HR=3.82, 95%CI: 1.90-7.67, p=0.0543) and Mib1 (p=0.0564) clone positive cell fractions also showed a strong trend towards reduced PFS.

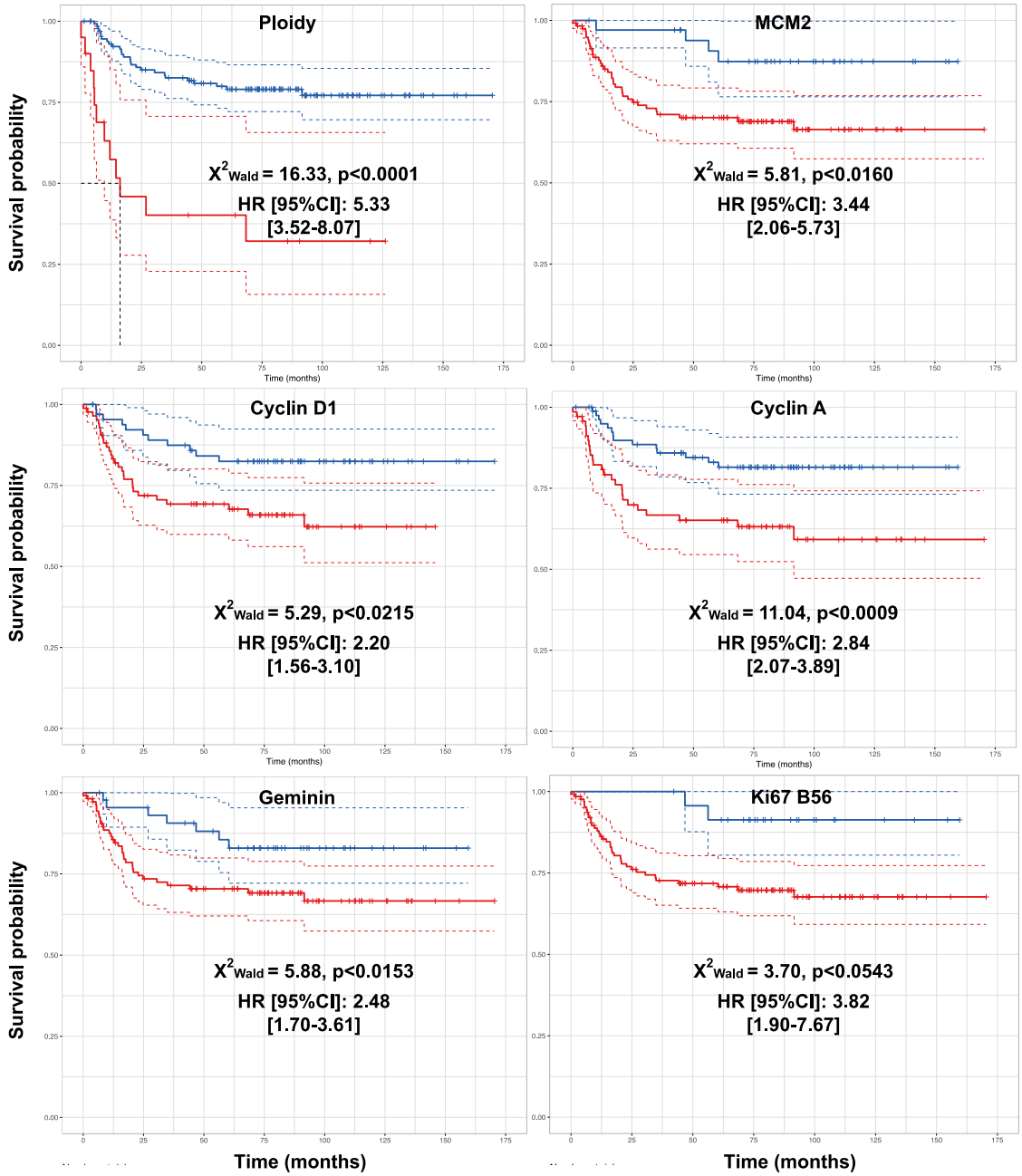

Figure 7. Kaplan-Meier plots based on univariate PWP gap time models of progression-free survival (N_{cases}=153; N_{PFS_events}=40) depicting cell cycle markers with the strongest associations. Negative (blue) vs. positive (red) represent the dichotomized expression levels at the respective median score of each marker. The Wald-statistics (χ^2), hazard ratios (HR) with 95% confidence interval (CI, dashed lines) are also shown. Censoring is indicated by "+". The figure is a slightly modified version of that in (92). It was used with permission of the publisher under the CC BY license.

4.2.4 Multivariable model selection for progression-free survival analysis

4.2.4.1 Standard multivariable survival models

For standard PWP survival models all possible combinations of cell cycle and clinical markers up to 5 variables were evaluated without testing for possible interactions among them. The AIC-based best multivariate prognostic model (AIC=271.6) included ploidy (HR=6.20, 95%CI: 2.89-13.30, p<0.0001), cyclin D1 (HR=2.27, 95%CI: 1.10-4.71, p=0.027) and MCM2 (HR=2.64, 95%CI: 0.86-8.08, p=0.090) while the second best model additionally included cyclin A. The top 10 multivariable PWP survival models are summarized in **Table 2**.

Table 2. Top 10 multivariable PWP-models using AIC-based model selection

Rank	Selected variables	Selection metric	Value
1	ploidy + MCM2 + cyclin D1	AIC	271.56
2	ploidy + MCM2 + cyclin D1 + cyclin A	AIC	271.84
3	ploidy + cyclin D1 + cyclin A	AIC	272.48
4	ploidy + cyclin D1	AIC	273.18
5	ploidy + MCM2 + cyclin D1 + geminin	AIC	273.30
6	ploidy + MCM2 + cyclin D1 + Ki-67 (B56)	AIC	273.36
7	ploidy + MCM2 + cyclin D1 + Ki-67 (Mib1)	AIC	273.38
8	ploidy + MCM2 + cyclin D1 + CDK2	AIC	273.41
9	ploidy + MCM2 + cyclin D1 + sex	AIC	273.41
10	ploidy + MCM2 + cyclin D1 + p21	AIC	273.42

4.2.4.2 Interaction models

We also tested all possible interactions between biomarkers to check whether their association with PFS and the signs of these effects would stay consistent across different expression levels of the markers. This also served as a methodological safety check to indirectly verify the blinded scoring values.

The highest-ranked interaction model (AIC=269.5) included ploidy (HR 5.6 8, 95%CI: 2.62-12.31, p<0.0001), MCM2 (p=0.61), cyclin D1 (HR 1.89, 95%CI: 0.88-4.09, p=0.11) and cyclin A (p<0.0001). To note that this model was the same as the second best performing standard model with a significant interaction between cyclin A and MCM2

($p<0.0001$), where the main effect of S-phase key marker cyclin A stayed significant ($p<0.0001$). Thus, it could be considered regardless of the interaction.

Survival curves of cell cycle phenotypes based on this best interaction model and corresponding predictions of progression hazards are presented in **Figure 8**. This model estimated similar HRs to the best standard multivariate model (**Subsection 4.2.4.1**) and also showed positive correlation between progressively increasing hazards for elevated cell cycle commitment (**Figure 8A**) and abnormal chromosome numbers (**Figure 8B**).

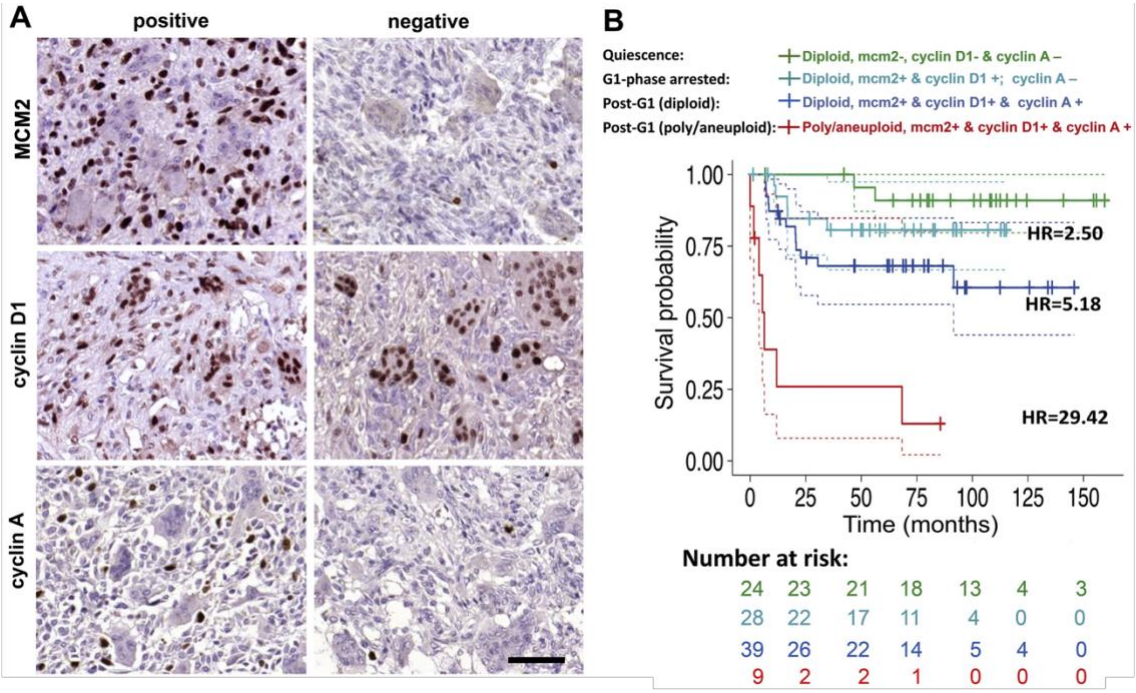

Figure 8. Combination figure based on the strongest interaction model including ploidy, MCM2, cyclin D1 and cyclin A with representative images of their immunoreactions (A) in positive and negative GCTB cases (DAB, brown; hematoxylin counterstain blue; scale bar: 50 µm) and Kaplan-Meier survival curves (B) showing PFS risk groups (N=100, N_{PFS_events}=27) based on cell cycle phenotypes of the mononuclear cell fractions. The survival characteristics of GCTB cases could be distinctly separated as the predicted hazard of progression was significantly positively associated with the increased proportion of S-G2 activity and mitotic disruption from G0/quiescent (diploid, MCM2, cyclin D1 and cyclin A negative; green, reference of HR=1.0), to G1-arrested (MCM2, cyclin D1 positive and cyclin A negative; light blue), to post-G1 (diploid post-G1-phase, cyclin A positive cases; dark blue), and to poly-/aneuploid post-G1 cases (dark red). The figure is reproduced with permission of the publisher (92) under the terms of the Creative Commons Attribution License (CC BY).

During sensitivity analyses (Table 3), after excluding 4 patients (2.6%) with incongruent (post-G1-phase i.e. cyclin A positive, yet licensing i.e. MCM2 negative) staining profiles, we found no relevant interaction regardless of the model building strategy. Interestingly, models that additionally included classical clinicopathological factors such as sex ranked 3rd (AIC=266.9) while the combination of the best model (ploidy, MCM2 and cyclin D1) with additional factors such as treatment type (rank 4; AIC=267.0), treatment and sex (rank 5; AIC=267.4), or age at first diagnosis (rank 9; AIC=267.6) ranked even lower and only emerged during sensitivity analyses (Table 3).

Table 3. Top 10 models of the sensitivity analysis

Rank	Selected variables	Selection metric	Value
1	ploidy + cyclin D1 + cyclin A	AIC	265.73
2	ploidy + cyclin A	AIC	266.91
3	ploidy + cyclin D1 + cyclin A + sex	AIC	266.93
4	ploidy + cyclin D1 + cyclin A + treatment	AIC	267.01
5	ploidy + cyclin D1 + cyclin A + treatment + sex	AIC	267.38
6	ploidy + cyclin D1 + cyclin A + Ki-67 (B56)	AIC	267.44
7	ploidy + cyclin D1 + cyclin A + geminin	AIC	267.45
8	ploidy + MCM2 + cyclin D1 + cyclin A	AIC	267.51
9	ploidy + cyclin D1 + cyclin A + age at diagnosis	AIC	267.64
10	ploidy + cyclin D1 + cyclin A + CDK2	AIC	267.66

4.3. Multinucleated giant cells

For the systematic analysis of GCs (**2. Objective: 2.**), a stratified random sample of 10-10 P and 1-Rec surgical cases was generated from the above cohort of 139 patients, who were investigated in (**2. Objective: 1.**) about cell cycle activity of mononuclear cell fractions and survival (92). These twenty cases (median age: 30.8 yrs, range: 13.7-76.6 yrs; 13 [65%] female) were then systematically assessed in at least three different osteoclast/GC rich high-power fields (HPF; 80x) (19). Confirming the random sampling, there was no relevant age difference (p=0.16) between sexes and between primaries and first recurrences (p=0.82). The median progression free survival was 58.1 months (range: 5-159.5, IQR: 18.9-79.2) during which 12 progression events occurred (**Subsection 4.1**). Although the median PFS was higher in P (70.7 months, IQR: 21.2-75.8) than in 1-Rec cases (40.2 months, IQR: 15.3-78.0), it was statistically not relevant ($p_{log\text{-}rank}$=0.36; $p_{Peto\text{-}Peto}$=0.55). Similarly, aggressive cases were more common among 1-Rec (n_{aggr}=4) than P (n_{aggr}=2) cases, whereas active (P: n_{act}=5; 1-Rec: n_{act}=4) and latent (P: n_{lat}=3; 1-Rec: n_{lat}=2) cases were somewhat more common among P than 1-Rec, however the association was non-relevant (p=0.73).

4.3.1. Nuclear characteristics of giant cells

Overall >1000 regions of interest (ROI) were evaluated with 18 cell cycle regulatory markers. The number of GCs (N_{GC}), GC nuclei (N_{GC_nuclei}) and respective cell cycle marker positive GC nuclei ($N_{GC\_nuclei+}$) were recorded and averaged for each case. To robustly estimate N_{GC} and N_{GC_nuclei} in a surgical specimen, their values were averaged over all tested cell cycle markers for each case, respectively. To use robust estimates, values of cell cycle marker positive GC nuclei ($N_{GC\_nuclei+}$) were normalized by calculating their ratio for each staining ($N_{GC\_nuclei+}/N_{GC\_nuclei}$).

Neither the overall average GC number (N_{GC}; p=0.53) nor the average number of GC nuclei (N_{GC_nuclei}; p=0.97) showed statistical difference between P and 1-Rec cases. There was a non-significant trend of inverse association between radiological grade (latent: L; active: A; aggressive: Ag) of GCTB and N_{GC} ($p_{L\_vs\_Ag}$=0.065; $p_{A\_vs\_Ag}$=0.11) and N_{GC_nuclei} ($p_{L\_vs\_A}$=0.093). The distribution of ratios of cell cycle marker positive GC nuclei in P and 1-Rec GCTB cases is summarized in **Table 4**.

Table 4. Ratios of cell cycle marker positive GC nuclei ($N_{GC\_nuclei+}/N_{GC\_nuclei}$).

Type of material	Marker	Ratio of positive GC nuclei				p	P^*_{adj}
		median	IQR	min	max		
P	CDK2	0.031	0.055	0	0.111	0.10	n.s.
1-Rec	CDK2	0.004	0.012	0	0.078		
P	CDK4	0.325	0.642	0	0.95	0.72	n.s.
1-Rec	CDK4	0.412	0.193	0.043	0.826		
P	cyclin A	0	0	0	0	0.17	n.s.
1-Rec	cyclin A	0	0	0	0.006		
P	cyclin D1	0.941	0.13	0.694	0.994	0.25	n.s.
1-Rec	cyclin D1	0.874	0.152	0.462	0.981		
P	cyclin G1	1	0.018	0.868	1	0.091	n.s.
1-Rec	cyclin G1	0.956	0.053	0.333	0.967		
P	geminin	0	0	0	0.005	**0.045**	n.s.
1-Rec	geminin	0.015	0.017	0	0.061		
P	Ki67 B56	0.027	0.045	0	0.096	0.32	n.s.
1-Rec	Ki67 B56	0.047	0.017	0.007	0.118		
P	Ki67 Mib1	0	0.012	0	0.048	**0.012**	n.s.
1-Rec	Ki67 Mib1	0.034	0.039	0	0.172		
P	Ki67 SP6	0.955	0.054	0	1	1	n.s.
1-Rec	Ki67 SP6	0.75	0.958	0.012	1		
P	MCM2	0.021	0.072	0	0.118	0.52	n.s.
1-Rec	MCM2	0.051	0.158	0	0.225		
P	MCM6	0.5	0.544	0.174	1	0.15	n.s.
1-Rec	MCM6	0.209	0.265	0.061	0.438		
P	$p15^{INK4b}$	0.773	0.162	0.447	0.967	1	n.s.
1-Rec	$p15^{INK4b}$	0.884	0.942	0	1		
P	$p16^{INK4a}$	0.032	0.045	0	0.233	0.69	n.s.
1-Rec	$p16^{INK4a}$	0.026	0.312	0.009	1		
P	$p21^{WAF1}$	0.818	0.162	0.264	1	0.31	n.s.
1-Rec	$p21^{WAF1}$	0.902	0.082	0.392	1		

Due to multiple testing (n=14), p-values were adjusted using the conservative Bonferroni correction (p^*_{adj}=0.0036). Bold p-values indicate non-adjusted significance at <0.05.

4.3.2 Licensing and general proliferation markers in giant cells

For the general proliferation marker protein Ki67, both Mib1 and B56 showed occasional positive reaction in a few GC nuclei (Figure 9A-B) while SP6 (Figure 9C) revealed weaker, but widespread reaction. Mib1 also showed weak to moderate cytoplasmic reaction in GCs. MCM2 was detected only in a few GC nuclei (Figure 9D), whereas

MCM6 was seen frequently, however, it was markedly weaker in large (>40 nuclei) GCs, than in smaller (<10-15 nuclei) ones or in mononuclear cells (**Figure 9E**). Though Mib1 positive nuclei in GCs were substantially higher (p=0.012) in 1-Rec than in P cases, it did not reach statistical significance after adjusting for multiple testing ($p^*_{threshold}$=0.0036). Similarly, none of the Ki67 clones (B56, p=0.32; SP6, p=1.0), neither MCM2 (p=0.52) nor MCM6 (p=0.15) positive GC nuclei showed statistically relevant differences between primary and recurrent samples (**Figure 9F**; **Table 4**).

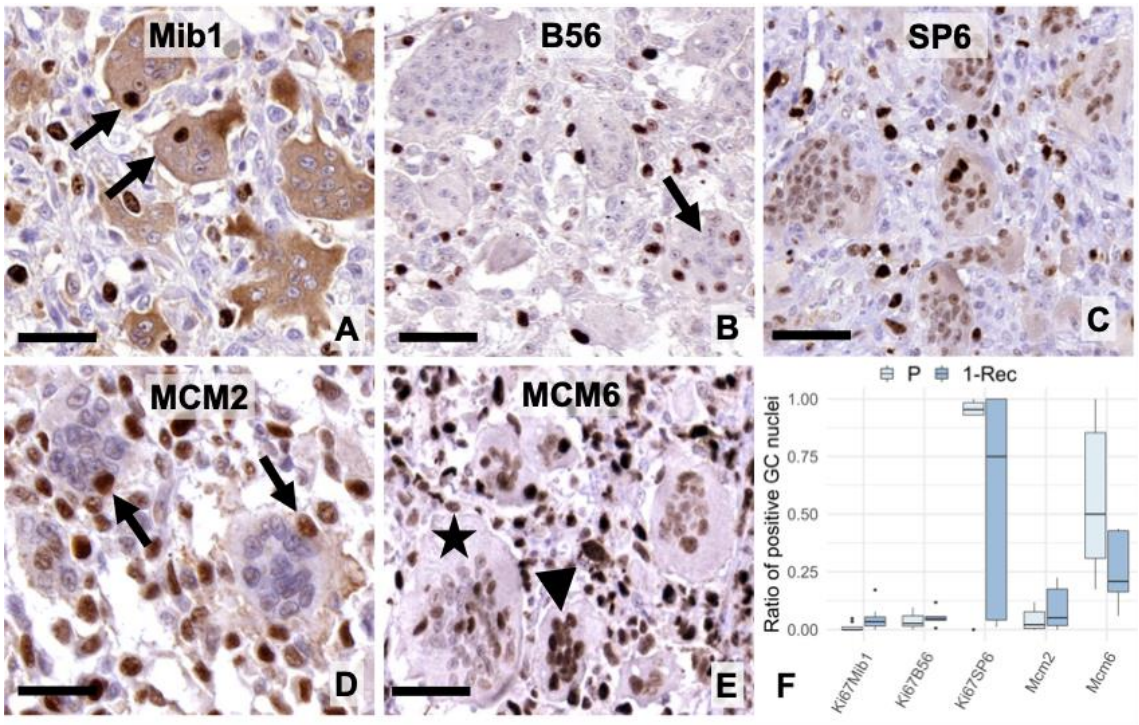

Figure 9. Expression of „general" proliferation markers Ki67 (A-C) and elements of the licensing hexamer MCM-complex (D-E) in GCs. The Ki67 antibody clones Mib1 (A) and B56 (B) showed only occasional nuclear positivity (arrows) while SP6 (C) revealed weaker, but widespread reactions in GCs. Cytoplasmic Mib1 positivity in GCs was also seen in most cases. MCM2 reaction (arrows) was rare (D). In contrast, MCM6 showed frequent nuclear positivity (E), which was more pronounced in smaller/younger (arrowhead), than in larger/aged GCs (star). Boxplot (F) of the quantified ratio of positive GC nuclei in primary (P) and first-recurrence (1-Rec) GCTB samples. DAB immunoperoxidase reactions (brown). Scale bars: A: 40 μm; B, C and E: 50 μm; D: 30 μm. The figure and its legend were slightly modified and reproduced with permission of the publisher (19) under the terms of the Creative Commons Attribution License (CC BY).

Interestingly, compared to mononuclear cell fractions engaged in the cell cycle (**Subsection 4.2.3**), in GCs only the increased average number of Ki67 Mib1 positive nuclei (HR=1.1, 95%CI: 1-1.2, $p_{non\text{-}adj.}$=0.041) was significantly associated with shorter PFS during univariate Cox proportional hazards analyses.

4.3.3 G1/S-phase progression markers in giant cells

CDK4 showed weak to moderate reactions in ~50% of GC nuclei (**Figure 10A**), concurrently most GC nuclei (median >87.5%) showed moderate to strong reaction with its G1 complexing partner, cyclin D1 (**Figure 10B**). The intensity of these reactions and the rate of cyclin D1 positive nuclei showed an inverse association with size and nuclear

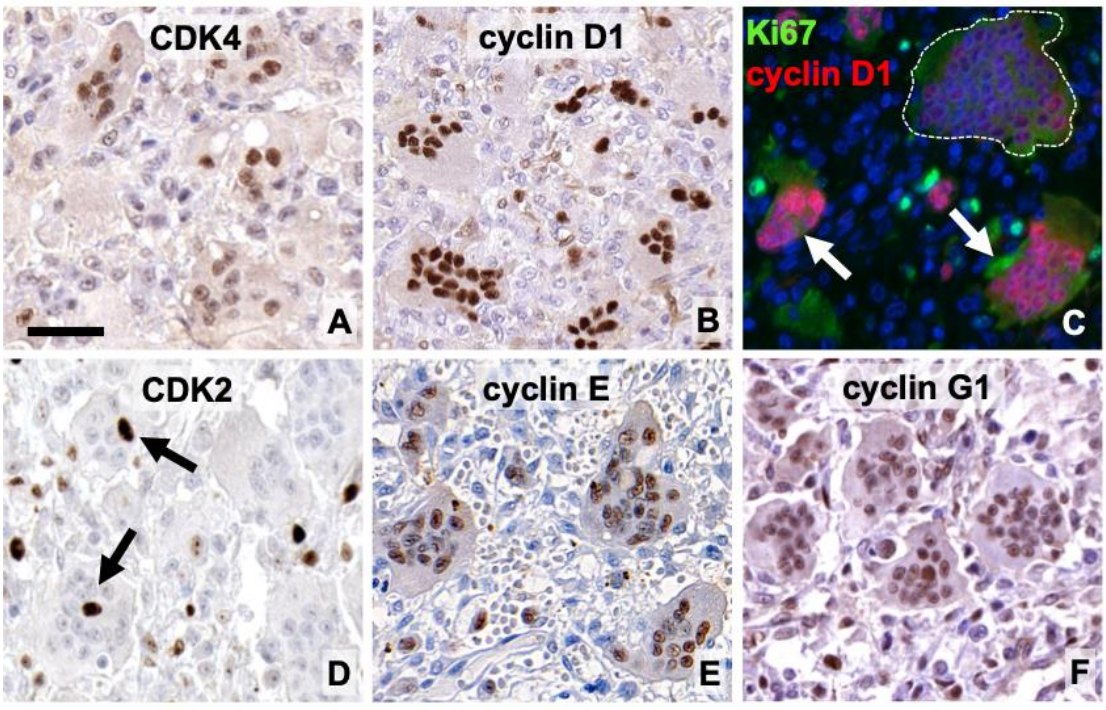

Figure 10. Expression of G1/S-phase cell cycle drivers in GCs. Several GC nuclei were positive for CDK4 (A) while virtually all stained positive for cyclin D1 (B). Double labeling (C) with Ki67 (green) and cyclin D1 (red). Cyclin D1 showed an inverse association with strong nuclear reaction in smaller GCs (white arrows) but only faint peripheral or missing central reaction in larger GCs (N_{GC_nuclei} >40; white dashed line). CDK2 (D) was rarely (<8%) detected (arrows). In contrast, its complexing partner cyclin E (E) demonstrated widespread expressions. Cyclin G1 (F) showed extensive (medians >95%) moderate reaction in GC nuclei, indicating its involvement in cell cycle arrest or rebound upregulation to control p53 overexpression and pro-apoptotic signaling. Scale bar: 40 μm. The figure was in part modified and reproduced with permission of the publisher (19) under the terms of the Creative Commons Attribution License (CC BY).

density of GCs (Figure 10C). After quantification, the nuclear positivity ratios of CDK4 (p=0.72) and cyclin D1 (p=0.25) did not show any relevant difference between P and 1-Rec cases. The G1-S-phase transition kinase CDK2 (Figure 10D) showed occasional positive nuclear expression, which did not differ statistically (p=0.10) between P and 1-Rec cases while its complexing partner cyclin E (Figure 10E; although not systematically counted) was widely detected in GC nuclei with a moderate reaction intensity. Cyclin G1 was widely detected in GC nuclei as a moderate reaction (Figure 10F). Its nuclear frequency in GCs showed a non-significant trend (p=0.091; Table 4) towards P cases.

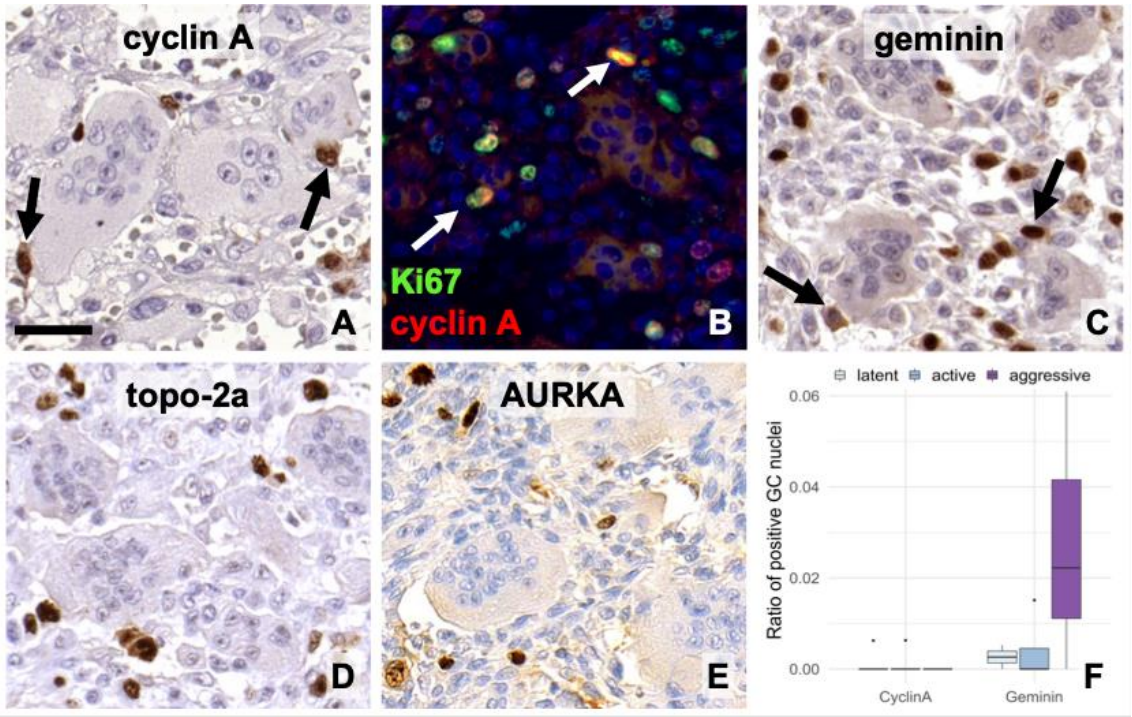

Figure 11. Expression of post-G1-phase cell cycle markers in GC (Section 4.3.4). None of the S-G2-M markers including cyclin A (A-B), repressor geminin (C), topoisomerase 2a (D) nor aurora kinase A (E) were detected in GC nuclei. Double immunolabeling (B) with Ki67 (green) and cyclin A (red) showed occasional co-activity (white arrows), however, only in mononuclear cells. Sporadically, cyclin A (A) and geminin (C) positive nuclei were observed adjacent to GC (black arrows), hinting at potential fusion of osteoclast precursors. Boxplot of ratio of cyclin A and geminin positive GC nuclei vs. Campanacci grades. DAB immunoperoxidase reactions (brown). Scale bar represents 30 μm on all images. Reproduced in part with permission of the publisher (19) under the terms of the Creative Commons Attribution License (CC BY).

4.3.4 Post-G1-phase markers in giant cells

Cyclin A (Figure 11A), the S-G2-M transition partner of CDK2, was seldom (<1%) detected in GCs but more likely in mononuclear cells (Figure 11B) and occasionally in fusing pre-osteoclasts (Figure 11A, C). The cell cycle repressor geminin (Figure 11C) was seen only at very low frequency (0-6%), although it appeared more often in 1-Rec cases (p=0.045, n.s.; Table 4). Topoisomerase 2a (Figure 11D), responsible for genome organization in S-phase and chromatid segregation in mitosis, was not detected in GCs. Also, as expected from these findings, both the G2-M-phase associated AURKA (Figure 11E) and primarily mitosis (metaphase-focused) pHH3 (not shown) were also missing from GCs. The latter was also very rare even in the mononuclear cell fraction.

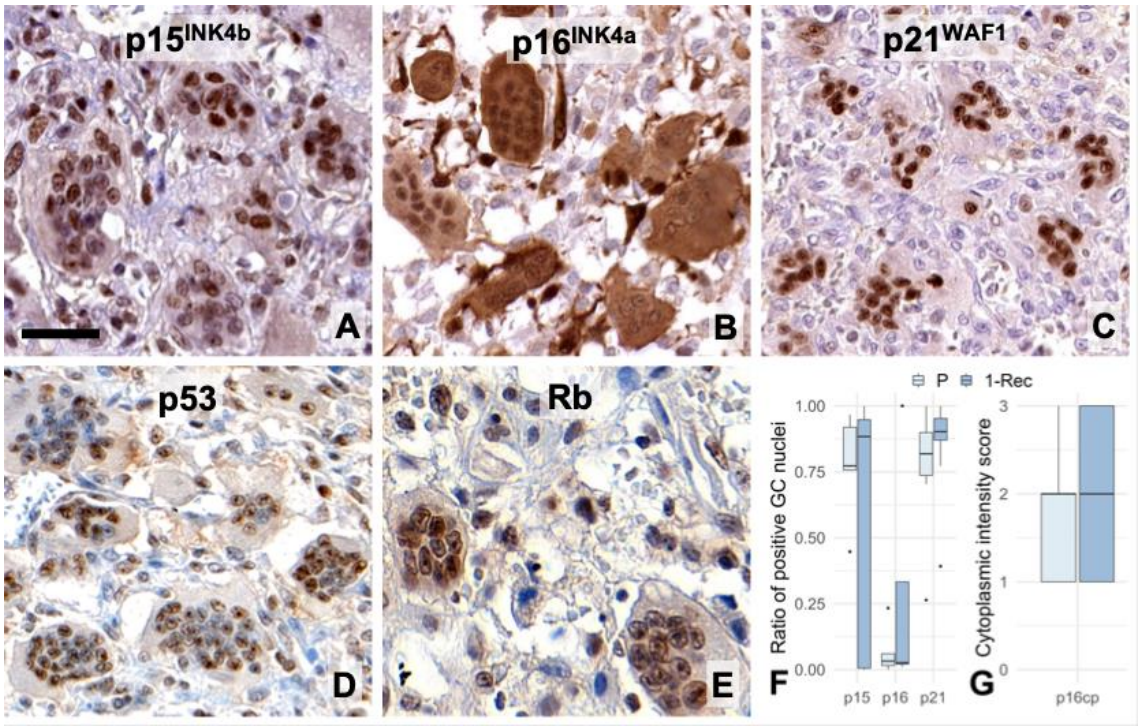

Figure 12. Expression of cell cycle control and inhibitory markers (Section 4.3.5). We found abundant nuclear reactions of $p15^{INK4b}$ (A) and $p16^{INK4a}$ (B), and also strong cytoplasmic staining with the latter (B). The general inhibitor $p21^{WAF1}$ (C), partly induced by p53 (D; DO7 clone), were both widely positive as they suppress both cyclin D1-CDK4/6 and cyclin E-CDK2 activity and block Rb (E) phosphorylation, thereby inducing G1-arrest and senescence. Boxplots (F) of the ratio of positive GC nuclei for (A-C); and for the cytoplasmic reaction of $p16^{INK4a}$ (G) in primary (P) and first recurrent (1-Rec) GCTBs. The figure was reproduced with permission of the publisher (19) under the terms of the Creative Commons Attribution License (CC BY).

4.3.5 Cell cycle inhibitors in giant cells

Corresponding to increased G1 and G1-S nuclear positivity, all CDK inhibitors (CDKI) tested including $p15^{INK4b}$, $p16^{INK4a}$, $p21^{WAF1}$ (**Figure 12A-C**) and $p27^{KIP1}$ were detected widely in GC nuclei. $p16^{INK4a}$ (**Figure 12B**) showed the least nuclear positivity but showed widespread cytoplasmic reaction, while $p21^{WAF1}$ (**Figure 12C**) was strongly detected practically in most GC nuclei.

Fitting into this pattern, most GC nuclei were immunopositive over a wide range of intensities for p53 (**Figure 12D**) and for retinoblastoma (**Figure 12E**). However, none of the systematically analyzed CDKI including $p15^{INK4b}$ ($p=1.0$), $p16^{INK4a}$ ($p=0.69$) and $p21^{WAF1}$ ($p=0.31$) showed differential expression between P and 1-Rec samples (**Figure 12F-G**; **Table 4**).

5. Discussion

5.1 Mononuclear cell fraction

Although GCTB is a rare tumor with primarily benign disease course, its locally aggressive osteolytic destruction and potential for pulmonary metastases (i.e. emboli, up to 7%), as well as for sarcomatous transformation (1-10%) and even fatal outcome (7, 10-13, 103-105), presenting in a young patient population (with peaks at the third and fourth decades), makes it clinically relevant (4, 7, 106-110). In addition, GCTB has a high recurrence potential (up to 75% depending on the treatment choice) (103), which is still poorly understood and cannot be sufficiently predicted from *a priori* clinicopathological parameters (21, 23, 92, 103, 111, 112).

As the cell cycle integrates the effects of both the dysregulated replication control and upstream growth signaling pathways (72), its accelerated progression is usually linked to less favorable outcome of tumor evolution (17, 50, 51). Previous studies investigating cell cycle activity in GCTB evaluated only smaller cohorts and did not (explicitly) evaluate survival, in particular, not considered repeated events within individual patients (46-48, 91).

Therefore, we performed *in situ* cell cycle analyzes in a large cohort of 154 surgical GCTB cases from 139 patients using DNA flow cytometry and immunohistochemistry focusing on the mononuclear cell fraction. Our comprehensive marker set revealed that while GCTB showed no major defect of cell cycle regulation, cases with elevated G1- and post-G1-phase mononuclear cell fractions had significantly increased hazard for shorter PFS. A major contribution of our work is linking cell cycle kinetics to survival characteristics using statistical analyses that explicitly incorporate and adjust for multiple recurrences and the increased probability of consecutive progression events.

Characteristic mutations in GCTB are point mutations of the *H3-3A* (formerly *H3F3A*) gene leading mostly to G34W alteration in the histone H3.3 protein of neoplastic stromal cells (17, 30, 113-116). Nonetheless, we could not detect histone H3 in its functional phosphorylated state (p-HistH3.3), which is required for chromatin condensation in mitosis. Amary et al. found that positive nuclear immunostaining with anti-H3F3A G43W rabbit monoclonal antibody was detectable in ~90% (213/235) of GCTBs but not in other 2928 cases including GCTB mimics (n=750) and various bone and soft tissue

tumors (n=2178) (28). They proposed that besides this immunopositivity (~85%, 11/13), subarticular localization were diagnostic markers for primary malignant GCTB (i.e. conventional GCT juxtaposed with high-grade sarcomas) and also for (giant-cell-rich) osteosarcomas (28).

Genomic instability was indirectly captured in our analyses through ploidy using DNA index calculated from flow cytometry (92). Poly- or aneuploid (13.0%) chromosomal setup showed a pivotal role in predicting future recurrences, as it was included into all top performing multivariate prognostic models and its presence alone increased hazard of progression or recurrence by a factor of six to eight. We and other groups reported chromosomal instability of GCTB stromal cells including frequent telomeric associations (50-70%), polysomies and individual cell aneusomies in association with tumor progression (14, 15, 21, 23-26).
Recently, Fittal et al. (29) investigated the methylation profiles of 17 GCTBs and found that benign (n=6) or indeterminate GCTBs (n=4) have no other driver mutations besides the canonical H.3.3 mutation, while malignant GCTBs (n=7) possessed additional genomic features resembling osteosarcoma (29). But compared to osteosarcomas, malignant GCTBs were enriched with mutations related to telomere dysfunction resulting in a TERT-mutated phenotype (5/7) or even elongated telomeres involving the alternative lengthening of telomeres pathway (ALT) or underwent loss of heterozygosity (2/7) at the RB1 locus. In their cohort, three of these seven malignant GCTBs were aneuploid with whole genome duplication, which occurred in adulthood but years prior to diagnosis but, notably, after the hallmark *H3-3A* (formerly *H3F3A*) mutation (17, 29). Likewise, in our cohort, all six cases (originating from five patients [3.6%]) either undergoing sarcomatous transformation after multiple recurrences (5/6; 83.3%) or presenting as a biphasic tumor with primary GCTB admixed with sarcoma at first presentation (1/6; 16.7%) were graded as aggressive (100%) and 4 (66.7%) were already aneuploid at the earliest specimen resection, representing 26% of all aneuploid cases (4/19).

Additional to ploidy, our multivariate PWP gap time models that considered the joint effect of multiple markers (94), also reinforced the pivotal role of MCM2, cyclin D1 and cyclin A, as the best panel for predicting PFS. Our study was the first to properly focus

on cyclin D1 expression in GCTB mononuclear cells in relation to survival. We found invers statistical correlation with PFS and cyclin D1 expression in GCTB mononuclear cells. To note that cyclin D1 occurred in all our top 10 multivariate models (**Table 2**). Its negative correlation with PFS stayed robust even after adjusting for the effect of ploidy and MCM2. In line with this, the most significantly differentially methylated regions between benign and malignant GCTBs were identified in the promoter region of the cancer driver gene *CCND1* encoding cyclin D1 (29). Earlier studies, which were performed only on a low number of cases (<40) with selected few markers, suggested that increased frequency of Ki67 (Mib1 clone) (18, 48), cyclin D1 and -D3 (46-48), as well as cyclin B1 (47) and the CDK4/6 inhibitor $p21^{WAF1}$ (46) positive mononuclear cells were significantly more common in recurrent and aggressive GCTB specimen. This was consistent with an accelerated cell cycle progression in the tumors of less favorable outcome, similar to more aggressive tumor entities like breast cancer and in melanomas (59, 71).

CDK4 and -6, the complexing partners of cyclin D1, were not identified as relevant prognostic factors in our analyses. In agreement with this, CDKIs blocking G1-S-phase transition were also nonessential, such as $p16^{INK4}$ specifically targeting CDK4/6 was not selected among any of the top 10 multivariate models (**Table 2**), while $p21^{WAF1}$ targeting both cyclin D1 and cyclin E-CDK complexes was included once into the 10^{th} ranked model (besides ploidy, MCM2 and cyclin D1). This imbalance suggested additional roles for cyclin D1 to Rb phosphorylation in neoplastic stromal cells, which might involve components of osteoclastogenesis (23). According to the classic view, the G1-S-phase transition is primarily initiated by D-type cyclins. But it has been challenged, as both *CDK4*- and *CDK6*-deficient mice were viable, even double knockout fibroblast could enter S-phase, though less frequently (63, 117). In recent phase III clinical trials, new generation of selective CDK4/6 inhibitors (palbociclib, ribociclib and abemaciclib) have demonstrated substantial overall- and progression-free survival benefits as add on therapies for patients with advanced-stage estrogen receptor (ER)-positive, ERBB2-negative (formerly human epidermal growth factor receptor 2, HER2) breast cancer (63, 118, 119). Besides biomarkers of treatment sensitivity (cyclin D1, *CDK2NA*), potential resistance to CDK4/6 inhibitors via rescue options like RB1 loss and ectopic overexpression of cyclin E-CDK2 can offer alternative pathways for G1/S progression

(118, 120). Breast cancer patients treated with CDK4/6 inhibitor palbociclib with high cyclin E1 mRNA expression had about halve the median survival (7.6 months) than those with low expression (14.1months). Also, changes of AURKA can result in enhanced G2-M-phase transition, which have been implicated as a resistance mechanism against CDK4/6 inhibitors (118, 121). AURKA exon inclusion was found as one of the most common transcriptional RNA machinery changes in H3.3 G34W mutated GCTB (114), although we have seen no relevant expression on the protein level.

The expression of cyclin A, a post-G1-phase marker, was tested for the first time by us in GCTB. It was included into the second-best ranked multivariate model (ploidy, MCM2, cyclin D1, cyclin A) for PFS prognosis based on all data and into the best model (ploidy, cyclin D1, cyclin A) during sensitivity analyses (**Table 3**). The complex of cyclin A and CDK2 promotes S-phase and DNA synthesis and controls the initiation of mitosis through activating the cyclin B1-CDK1 complex by orchestrating their centrosomal and nuclear functions (71, 92). Though, neither MCM2 nor cyclin A was an independent, significant predictor variable in the model, their inclusion offered a better coverage of the cell cycle and could significantly improve the overall model performance and robustness in terms of AIC values (92). Due to independent, blinded scoring, cyclin A helped in identifying potential scoring errors. In the multivariate interaction model, it enabled the automatic detection of cases with incongruent staining profiles e.g., S-G2 progressed (cyclin A positive) yet non-licensed (MCM2 negative) mononuclear cell fractions, which only occurred in four cases (2.6%).

Furthermore, our cluster analysis revealed that licensing-related MCM2 levels showed higher correlation with S-G2-M drivers such as cyclin A and the late cell cycle repressor geminin (49, 52, 59, 73, 122) than with the G1-S-phase catalyzers cyclin D1 and CDK4, implying that there is no major defect of cell cycle regulation in mononuclear cells (50, 51, 73). Hence, emergence of cyclin A (76, 120, 123) in the panel allowed for reliable identification of both the S-G2-M-phase cell fractions and the G1-phase arrested (MCM2 and cyclin D1 positive but cyclin A negative) cases. The central role of cyclin A in DNA synthesis and post-G1- phase was emphasized by its presence in all the top 10 models during sensitivity analyses (**Table 3**) (62, 124). Similar findings were published in high-grade osteosarcoma that patients with cyclin A overexpression showed elevated risk for

relapse (125) and in melanoma where increased cyclin A positive cell fractions differentiated them from dysplastic nevi (71).
Geminin, also an indicator of G2-M-phase cells, has been reported too as a marker of tumor progression and adverse prognosis in colon (126) and breast cancers (122), as well as in high-grade astrocytomas (127) and oligodendroglial tumors (128). In our study, it served as a somewhat less prominent alternative to cyclin A. Notably, most (>90%) geminin positive cases were also cyclin A positive, despite our independent blinded scoring.

Interestingly, clinical variables emerged only during sensitivity analyses (**Table 3**) as non-significant but still relevant predictors. Although the effect of surgical treatment radicality on PFS was less pronounced compared to cell cycle regulatory proteins (ploidy, cyclin D1 and -A) and sex, it emerged as one of the main predictors for PFS (112, 129, 130) during multivariate sensitivity analyses (4^{th} and 5^{th} model; **Table 3**). Though the surgical treatment approach was a non-significant predictor in our cohort, it could stabilize and improve the model fit in certain cases. A large retrospective Chinese cohort study, based on simple Cox survival models of the next recurrence event, reported similar findings that PFS was significantly lower after curettage than after (more radical) wide resection (130). They also reported shorter survival for younger (<30 yrs) than older (>30 yrs) patients (130). Although the median age was quite similar (31 yrs) in our cohort, we could not verify this age threshold. In a subset (n=32, 2.3%) of another large Chinese cohort (n=1365) that investigated differences between 12 primary and 20 secondary malignant GCTBs, found a similar mean age of 33.7 yrs and a 5-year survival rate of 56% and 40%, respectively (11). They have also emphasized the importance of adequate surgical margins, which significantly reduced local recurrence rates. The median RFS of 61.5 months of secondary malignant tumors was significantly longer compared to 19 months of benign GCTBs (11). The authors identified ~4 years (49.5 months) as a critical ROC/AUC-threshold for suspicious recurrence and secondary transformation of GCTBs (11). In contrast, in our cohort, the RFS rate of GCTBs with post-G1/aneuploid mononuclear cell cycle phenotypes at 50 months (**Figure 8B**) was considerably lower at 22% (n=2/9), hinting at the additional utility of cell cycle profiling.

A limitation of our work was that all our survival analyses were explorative and performed by fitting the full data set. Therefore, the proposed models require proper external validation (99, 131-136). Furthermore, the investigated cohort predates the approval of RANKL inhibitors and their application to GCTB as denosumab, a fully human monoclonal antibody against RANKL, was first approved in 2013 (109, 137, 138). *In vitro* studies showed that although denosumab reduces the proliferative rate of stromal cells, it has no cytotoxic effect (137). Also, it primarily targets GCs, but only functionally inhibits them. Therefore, "crude" OS and PFS rates derived from our study could serve as baselines for estimating the risk of recurrence if patients were treated only surgically (11, 13, 112). Recently, surgical technique became even more relevant, as it has been suspected that longer (>4-6 months) neoadjuvant denosumab therapy might increase the risk of local recurrence in patients treated with curettage (109, 137-140). As denosumab increases osteoclast maturation and concurrently the (re-)mineralization of initial tumor margins (116, 137), it traps mononuclear tumor cells and GCs within (139), which consequently cannot be sufficiently resected during less radical surgery (104, 105). Furthermore, it can induce post-therapeutic changes that resemble high-grade osteosarcoma (23, 108, 141).

Mahdal et al. identified a specific receptor tyrosine kinase signaling pattern of stromal cells involving the platelet-derived growth factor receptor β (PDGFRβ) (140) that when blocked with a selective inhibitor (sunitinib), reduced viability of these neoplastic cells. Thus, PDGFRβ is emerging as a potential target for combination therapy using sunitinib and denosumab to limit GCTB recurrences (140). Recently, Antal et al. investigated this in a small case series of five GCTB samples (139). They observed an inverse expression pattern of PDGFRβ on stromal cells, as it increased during denosumab treatment and decreased in recurrent tumors after its discontinuation, which supports the previously suggested synergistic effect of sunitinib when combined with denosumab (139, 140).

Furthermore, most recently, Venneker et al. identified histone deacetylase (HDAC) inhibitors as potential compounds primarily targeting the neoplastic stromal cell population based on the hallmark histone H.3 (*H3-3A*, formerly *H3F3A*) G34W mutation of GCTB using cell lines and 2D and 3D *in vitro* models (115).

5.2 Multinucleated giant cells

Earlier studies of GCTB showed the widespread expression of cyclin D1 (37, 46-48, 91) cyclin D3 (47) and $p21^{WAF1}$ (46), and less frequently of $p16^{INK4a}$ and scarcely of Ki67 (37) in GCs. Nonetheless, these data were considered insufficient to unequivocally declare replication activity in GCs (16, 23). Therefore, we performed comprehensive quantitative analyses whether cell cycle regulation can be linked to GC formation and activity (**Figure 13**) as well as clinical phenotype of GCTB (19). We not only confirmed these previous observations, but also revealed additional cell cycle promoters (48) that confirmed an early cell cycle commitment in GCs. However, the effect of the generally detected cell cycle licensing MCM6, G1/S-phase transition drivers CDK4 and cyclin E, are probably counteracted in GCs by upregulated CDKIs, such as $p15^{INK4b}$, $p16^{INK4a}$, $p27^{KIP1}$ and $p21^{WAF1}$, likely induced by the p53 tumor suppressor pathway, which is consistent with an arrested cell cycle in late G1-phase (**Figure 13**).

Ki67 has been widely accepted as a validated proliferation marker for various human cancers (142, 143). It has multiple functions and time-dependent expression levels that are tightly coupled to cell cycle phases and time spent in G0/quiescence (144). During interphase, it is required for normal cellular and nucleolar distribution of heterochromatin (145), and for the inhibition of p21-mediated G1/S-phase checkpoint activation. At the start of mitosis, Ki67 relocalizes to form perichromosomal protein sheaths to prevent aggregation of mitotic chromosomes and remains until nucleus reformation in G1 (142, 143). It has been generally accepted that Ki67 (Mib1 clone) is confined to mononuclear cells in GCTB (146). There was only one study that reported semi-quantitative results about a weak Ki67 Mib1 staining in <5% of osteoclast-type GCs in only 3 out of 29 (10%) samples, which comprised of 27 GCT of tendon sheath and only 2 GCTBs (37). Interestingly, in this study foreign body-type GCs showed similar (<5%) Ki67 Mib1 intensities to osteoclast-type GCs, but more commonly in 14 out of 51 (27.5%) samples (37). Similarly, we found that both Mib1 and B56 clones of Ki67 showed a low ratio of nuclear positivity (<10%) while SP6 demonstrated a wide range with a median of >75%. Ki67's tight association to mitosis and time spent in G0/quiescence, might serve as a prognostic marker in GCTB. In our explorative univariate survival analysis, the higher ratio of positive Ki67 Mib1 GC nuclei in 1-Rec vs. P cases was linked to shorter PFS.

The prominent cytoplasmic Mib1 staining in GCs (**Figure 9A**) was also described by others (146). It is likely to be related to metabolic elimination of Ki67 by the ubiquitin proteasome system (143). The differential occurrence of Ki67 clones can be in part caused by the slower degradation of the epitope region recognized by SP6 compared to the others (145, 147).

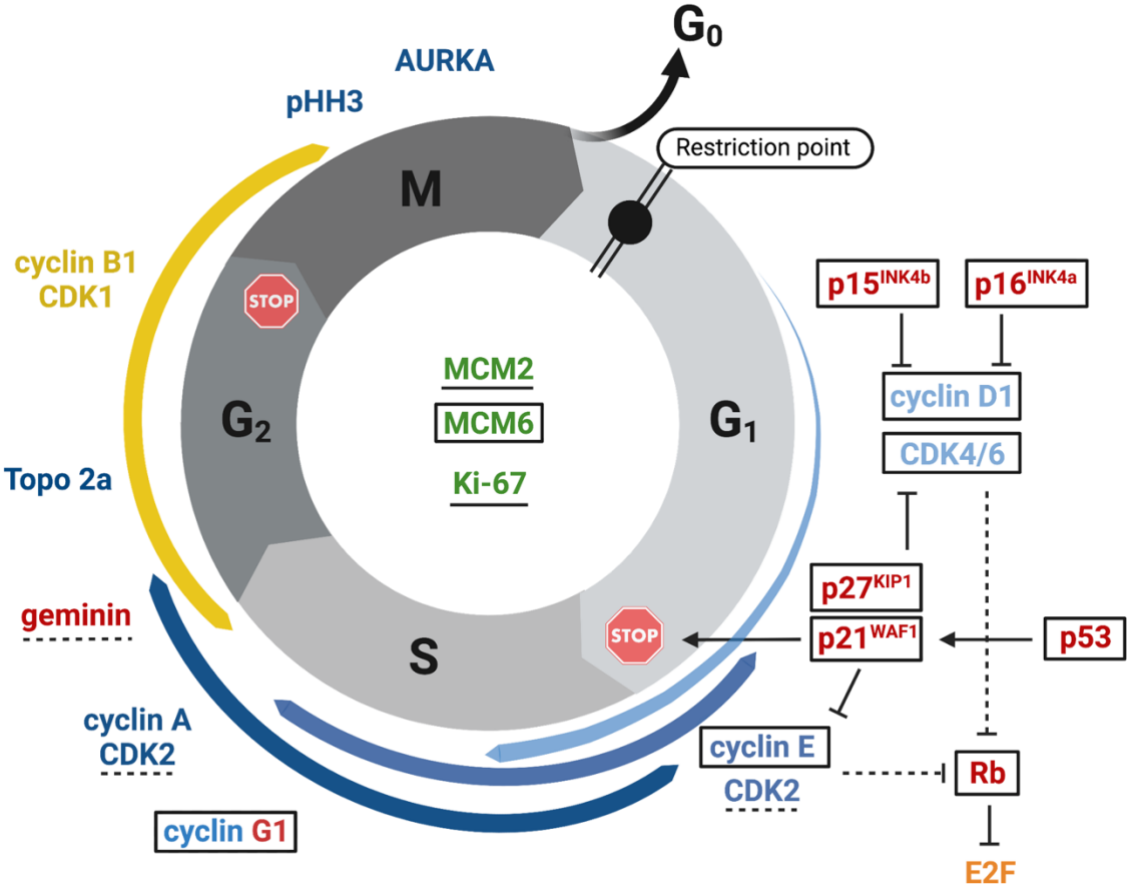

Figure 13. Investigated cell cycle regulatory proteins in giant cells. Arrows indicate activating- while "T" signs represent inhibitory functions. General proliferation markers in green can be detected during the whole cell cycle; cyclin-CDK pairs in shades of blue support G1-S and S-G2-M transitions. Markers in red depict inhibitors. cyclin G1 was written in blue-red letters to indicate its potential dual role as either oncopromoter or suppressor. Cyclin B-CDK1 (yellow) were not evaluated systematically in our projects. In GCs, the framed markers were widely detected, those underlined with continuous (MCM2, Ki-67) or dashed lines (CDK2, geminin) were expressed rarely or very rarely, respectively; while those which are not labeled either of these ways, were practically not detected. Colored ribbons show the expression duration and extent of the matching-colored cyclin-CDK complexes. The image and its legend were modeled after figures in (19) under the terms of the Creative Commons Attribution License (CC BY). It was created with BioRender.com.

Members of the MCM2-7 helicase complex (**Figure 13**) are required for the controlled licensing and duplication of DNA (148). Thus, components of the licensing complex can be detected during the whole cell cycle until the exit to G0 (51, 52, 59). However, while MCM6 is involved in relaxing DNA to single strands, the MCM2 subunit, has potential inhibitory effect on this function (58). Our widespread detection of MCM6 with moderate intensity but only occasional occurrence of MCM2 in GC nuclei, may reflect the initiation of DNA unwinding in GCs. Upregulated RNA expression of MCM6 and mitotic regulators like cyclin B1 and CDK1 has been linked to toll-like receptor 2 (TLR2) signaling driven escape of p53-dependent DNA damage response and consequent granuloma-resident macrophage differentiation and polyploid progeny generation in the presence of persistent inflammatory stimuli (36).

We revealed the widespread emergence not only of (the previously detected) cyclin D1 (46, 47), but also its partner CDK4 in the earliest G1-S phase promoter complex (**Figure 13**). Their complex also supports the activation of consecutive G1-S-transit promoters cyclin E-CDK2 by reducing mitochondrial metabolism to prevent cyclin E degradation (149). In agreement with this, we regularly detected cyclin E, however, only very rarely found its complexing partner CDK2 in GC nuclei. This either indicates a late G1-arrested cell cycle (19) or might be correlated with CDK2-independent S-phase entry (150), which is driven by cyclin E (123). For the latter, the centrosomal localization signal of cyclin E is needed, as it facilitates the kinase-independent loading of MCM helicase (particularly MCM2) onto chromatin through physical interaction with CDT1 and the MCM complex (52, 151). Cyclin E overexpression can also induce chromosomal instability involving breaks and translocations (123, 152). This effect can be potentiated by p53 deficiency to accelerate tumorigenesis (149, 152). Additionally, the cyclin D-CDK4/6 axis also links proliferation to cell growth by simultaneously driving Rb phosphorylation and E2F release (153) as well as metabolic activity by promoting cell growth through the mammalian target of rapamycin complex 1 (mTORC1) pathway (54, 154).

Besides cell cycle progression and tumorigenesis, cyclin D1 has multiple roles depending on its form concerning various cellular functions, such as cellular migration, -invasion, and mitochondrial metabolism, which might also play a role in GC differentiation and growth (149). In its DNA-bound form, cyclin D1 regulates noncoding genome expression affecting more than 30 transcription factors and their activity (155) including key tumor

suppressors like p53, E2F and the interplay between estrogen receptors and BRCA1 in breast cancer (149, 156). Furthermore, cyclin D1 can induce chromatin remodeling and consecutive chromosomal instability (149), hence, it is thought to be necessary for multinucleate GC formation (46, 47, 149). This corresponds to findings in cardiomyocytes of transgenic mice that overexpressed cyclin D1 resulting in abnormal patterns of multinucleation (157). Similarly, cyclin D1 was only detected in giant- but not in diploid trophoblasts and its expression preceded the initiation of trophoblast differentiation (158). In a cohort of 32 GCTB cases, Kauzman et al. reported low-level cyclin D1 gene amplifications in ~2/3 of the samples while at the protein level, expression of both cyclin D1 and -D3 was predominant in GC nuclei, implying a potential link with the pathogenesis of GCTB (47). The same group has also described higher cyclin D1 and associated $p21^{WAF1}$ expressions in GC nuclei in a small cohort of altogether 16 primary and recurrent cases (46).

$p21^{WAF1}$ is considered to be one of the main effectors of p53 driven replication stress-, DNA damage response, DNA repair and even apoptosis signaling (159, 160). In such cases, $p21^{WAF1}$ initiates either the arrest of G1/S-transition by inhibiting cyclin D1-CDK4/6 complex and CDK2 at the G1-checkpoint (159), or hinders G2/M transition by blocking cyclin B1-CDK1 complexes and inflicting G2 arrest (161). The former pathway, paradoxically, may also be important for CDK4/6 complex assembly (162) and for the nuclear export of cyclin D1 (163, 164). These might explain our frequent detection of CDK4 but not CDK2, and the high levels of cyclin D1 in GC nuclei. While the latter p53/p21-associated blockage of mitotic bypass triggers senescence in tetraploid (4N) G1 state (33, 83, 161). This is accompanied by the early degradation of cyclin B1 and other mitotic regulators, thus rendering cells incapable of the G2/M transit (161). This irreversible G2 arrested state is similarly characterized by the accumulation of cyclin D1 and the lack of G2/M markers, particularly cyclin B1 (161, 165). This marker profile corresponded to our findings, as neither cyclin B1 nor M-phase related AURKA and pHH3 nor any tested S-G2-M-phase markers including cyclin A, topoisomerase 2a, and repressor geminin were detected within GCs. However, leaning towards CDKI induced G1 arrest, Rb was also upregulated in GC nuclei in our series. The crucial role of CDKIs, $p21^{WAF1}$ and $p27^{KIP1}$ in bone metabolism, especially in osteoclast differentiation and

function was further demonstrated in double knockout mice as these animals suffered from osteopetrosis (166).

The upregulation of other CDKIs, selectively targeting CDK4/6 proteins including $p15^{INK4b}$ and $p16^{INK4a}$, further supports their cell cycle-related activity in GCs (167, 168). The induction of $p16^{INK4a}$ activity occurs after p21-mediated cell cycle arrest (63, 169, 170). Thus, $p16^{INK4a}$ upregulation further stabilizes the terminal stages of replicatory arrest and induces the terminal state of senescence (169). $p16^{INK4a}$ achieves this either by directly blocking the cyclin D-binding domain and catalytic activity of CDK4 (169) or by disrupting the cytoplasmic, post-translational folding of CDK4 (171), which is required for CDK4's functional activation (63). This might explain the strong, diffuse cytoplasmic staining that we have seen with $p16^{INK4a}$ in GCs (**Figure 12B**). Senescence also promotes cell maturation and the development of complex senescence-associated secretory phenotypes (SASP) (54, 170) that might in turn change the tissue microenvironment and further promote tumor progression (170). Accordingly, in GCTB giant cells, senescence is probably interlinked with the production of key proteases of bone resorption like cathepsin K and matrix metalloproteinase-9 (MMP-9) (172-174). Furthermore, $p16^{INK4a}$ might also be associated with the aged-cell decay in GCs (175).

Previous to our work, hardly a few publications concerned with the expression of the genomic guardian, p53, in GCTB mononuclear and giant cells (91, 176, 177). We elaborated upon p53 expression in GCTB by using two different antibody clones (DO7 and BP53-12) and provided clear evidence that most GCs upregulate p53. This might result from the aforementioned complex interplay of pathways involved in cell growth, differentiation and chromatin restructuring coupled with multinucleation driven by cyclin D1, -E and $p21^{WAF1}$. We were the first to detect an additional p53 target, cyclin G1 in GCTB (19). It has dual functions that can be involved in both cell cycle arrest and accelerated S-G2-M progression. As an oncogene, cyclin G1 can initiate the autoregulatory feedback loop between p53 and E3 ubiquitin-protein ligase (MDM2) (84, 85, 87). For this, cyclin G1 recruits Ser/Thr protein phosphatase 2A (PP2A), which dephosphorylates and activates MDM2 (86). In turn MDM2 represses p53 in multiple ways: by binding to its transactivation domain, by allowing its nuclear export and by promoting p53's proteasomal degradation through its ligase activity (178, 179). We

detected almost ubiquitous cyclin G1 expression in most GC nuclei with a non-significant trend towards slightly reduced ratios in 1-Rec (median 95.6%) vs. in P (median 100%) GCTB cases, which rather suggest that cyclin G1 upregulation is a rebound effect to control p53 overexpression and to prevent apoptosis (84, 86, 87).

We have seen cell cycle marker expression profiles that reflected the maturation dynamics and age-related activity of GCs (48). *In vitro* data confirm an inverse correlation between GC size and resorption activity in acidic conditions (180). Similarly, we found a negative association between the average size of GCs, their nuclear density and the Campanacci grade of GCTB. Emphasizing the key role of cyclin D1, Lujic et al. reported that cyclin D1 expression in GCs containing <15 nuclei was statistically associated with tumor recurrence, achieving the highest hazard (HR~8) in standard multivariate Cox and logistic regression models while being the only other significant prognostic marker besides mononuclear p53 positivity (91). Qualitatively, we also observed that cyclin D1 (**Figure 10C**) and MCM6 reactions were markedly stronger and more frequent in small sized (<10-20 nuclei) than in larger GCs (48), especially if N_{GC_nuclei} was >40. This was in line with our earlier findings of lower average size of GCs in recurrent GCTB cases where the growth-related EGFR protein level was elevated in stromal cells, driving GC formation and activity (6). All these imply that smaller sized GCs are the younger, dynamically forming population (**Figure 2**), which may show more signs of early replication than aged, functionally less active and oversized GCs with gradually degrading protective function of cyclin D1. To note, however, that we could not assess the modifying effect of RANKL inhibitors on GC maturation and cell cycle related nuclear activity.

6. Conclusions

In conclusion, through the comprehensive coverage of the cell cycle machinery including several progression markers first detected systematically here, we could i) identify a marker panel including ploidy and elevated replication licensing (MCM2), G1-phase (cyclin D1) and post-G1-phase (cyclin A) positive mononuclear cell fractions, which can assist in identifying GCTB patients with increased hazard of progression; and ii) verify early replication activities in GCs and confirm the pivotal role of cyclin D1-CDK4/6 axis while elaborating their complex interplay with the p53-p21 effector pathway and other CDK inhibitors, which together induce G1 arrest and secretory senescence to support the functional maturation, survival and activity of GCs in GCTB.

This restricted immunochemistry panel of these three cell cycle markers and ploidy can all be detected at reasonable costs *in situ* and with flow cytometry, which are readily available methods in centers of soft tissue and bone pathology. Our approach can be exploited to concurrently profile mononuclear and giant cells and to identify GCTB patients with higher risk of recurrence for whom more careful follow up and/or adjuvant RANKL inhibitor- or bisphosphonate treatment may additionally be required. Furthermore, our findings may support the adoption of selective CDK4/6 inhibitors or other novel therapeutic approaches to GCTBs in the future.

7. Summary

In this doctoral research project, by using a comprehensive set of cell cycle markers, we studied if 1) cell cycle fractions within the mononuclear cell compartment of GCTB can predict its progression-free survival and 2) looked for potential replication activities in GCs to investigate whether these have diagnostic or clinical relevance in GCTB.

In mononuclear cells, unsupervised cluster analysis showed no major defect of the cell cycle. But PFS was significantly negatively associated in univariate analyses with DNA index (poly-/aneuploidy) and elevated post-G1/S-phase markers cyclin A, repressor geminin and early replication proteins MCM2, cyclin D1 and Ki67 B56 positive mononuclear cell fractions. The best multivariate prognostic survival model combined ploidy, and the proportion of MCM2, cyclin D1 and cyclin A positive mononuclear cells. After validation, this restricted panel might be utilized in the clinical setting for treatment and follow-up planning to identify GCTB patients with increased hazard of recurrence and progression.

In multinucleated GCs, the general upregulation of early pro-proliferative markers MCM6, CDK4 and cyclin E, coupled with the widespread, age-dependent expression of cyclin D1, unequivocally demonstrated an early (G1-S-phase) replication activity. However, these were counteracted by the pervasive expression of CDK inhibitors, primarily by the p53-induced $p21^{WAF1}$ and possibly by p53-cyclin G1 pathways and got further stabilized by selective CDK4/6 inhibitors ($p15^{INK4b}$, $p16^{INK4a}$) resulting in G1 arrest and consequent state of secretory senescence. This was also confirmed by the missing detection of post-G1 markers (such as cyclin A, geminin, topoisomerase 2a, pHH3 and AURKA). The complex interplay of these G1-S-phase markers was consistent with lacking DNA replication and seemed to be required for multinucleation, differentiation, functional maturation, and bone resorbing activity of GCs in GCTB.

8. References

1. WHO Classification of Tumours Editorial Board. WHO classification of tumours, 5th edition: Soft Tissue and Bone Tumours. Vol. 3. International Agency for Research on Cancer, Geneva, 2020: 440-447.
2. Fletcher CD. (2014) The evolving classification of soft tissue tumours - an update based on the new 2013 WHO classification. Histopathology, 64: 2-11.
3. Turcotte RE. (2006) Giant cell tumor of bone. Orthopedic Clinics of North America, 37: 35-51.
4. Szendröi M. (2004) Giant-cell tumour of bone. J Bone Joint Surg Br, 86: 5-12.
5. Balke M, Schremper L, Gebert C, Ahrens H, Streitbuerger A, Koehler G, Hardes J, Gosheger G. (2008) Giant cell tumor of bone: treatment and outcome of 214 cases. Journal of cancer research and clinical oncology, 134: 969-978.
6. Balla P, Moskovszky L, Sapi Z, Forsyth R, Knowles H, Athanasou NA, Szendroi M, Kopper L, Rajnai H, Pinter F, Petak I, Benassi MS, Picci P, Conti A, Krenacs T. (2011) Epidermal growth factor receptor signalling contributes to osteoblastic stromal cell proliferation, osteoclastogenesis and disease progression in giant cell tumour of bone. Histopathology, 59: 376-389.
7. Bertoni F, Bacchini P, Staals EL. (2003) Malignancy in giant cell tumor of bone. Cancer, 97: 2520-2529.
8. Rock MG, Pritchard DJ, Unni KK. (1984) Metastases from histologically benign giant-cell tumor of bone. J Bone Joint Surg Am, 66: 269-274.
9. Rock MG, Beabout JW, Unni KK, Sim FH. (1984) Malignant giant cell tumor of bone. Orthopedics, 7: 909-913.
10. Vari S, Riva F, Onesti CE, Cosimati A, Renna D, Biagini R, Baldi J, Zoccali C, Anelli V, Annovazzi A, Covello R, Ascione A, Casini B, Ferraresi V. (2022) Malignant Transformation of Giant Cell Tumour of Bone: A Review of Literature and the Experience of a Referral Centre. International journal of molecular sciences, 23: 10721.
11. Liu W, Chan CM, Gong L, Bui MM, Han G, Letson GD, Yang Y, Niu X. (2021) Malignancy in giant cell tumor of bone in the extremities. Journal of Bone Oncology, 26: 100334.

12. Palmerini E, Picci P, Reichardt P, Downey G. (2019) Malignancy in Giant Cell Tumor of Bone: A Review of the Literature. Technology in Cancer Research & Treatment, 18: 1533033819840000.
13. Domovitov SV, Healey JH. (2010) Primary Malignant Giant-Cell Tumor of Bone Has High Survival Rate. Annals of Surgical Oncology, 17: 694-701.
14. Moskovszky L, Dezso K, Athanasou N, Szendroi M, Kopper L, Kliskey K, Picci P, Sapi Z. (2010) Centrosome abnormalities in giant cell tumour of bone: possible association with chromosomal instability. Mod Pathol, 23: 359-366.
15. Balla P, Maros ME, Barna G, Antal I, Papp G, Sapi Z, Athanasou NA, Benassi MS, Picci P, Krenacs T. (2015) Prognostic impact of reduced connexin43 expression and gap junction coupling of neoplastic stromal cells in giant cell tumor of bone. PLoS One, 10: e0125316.
16. Knowles HJ, Athanasou NA. (2009) Canonical and non-canonical pathways of osteoclast formation. Histol Histopathol, 24: 337-346.
17. Behjati S, Tarpey PS, Presneau N, Scheipl S, Pillay N, Van Loo P, Wedge DC, Cooke SL, Gundem G, Davies H, Nik-Zainal S, Martin S, McLaren S, Goody V, Robinson B, Butler A, Teague JW, Halai D, Khatri B, Myklebost O, Baumhoer D, Jundt G, Hamoudi R, Tirabosco R, Amary MF, Futreal PA, Stratton MR, Campbell PJ, Flanagan AM. (2013) Distinct H3F3A and H3F3B driver mutations define chondroblastoma and giant cell tumor of bone. Nat Genet, 45: 1479-1482.
18. Antal I, Sapi Z, Szendroi M. (1999) The prognostic significance of DNA cytophotometry and proliferation index (Ki-67) in giant cell tumors of bone. Int Orthop, 23: 315-319.
19. Maros ME, Balla P, Micsik T, Sapi Z, Szendroi M, Wenz H, Groden C, Forsyth RG, Picci P, Krenacs T. (2021) Cell Cycle Regulatory Protein Expression in Multinucleated Giant Cells of Giant Cell Tumor of Bone: do They Proliferate? Pathol Oncol Res, 27: 643146.
20. Wulling M, Engels C, Jesse N, Werner M, Delling G, Kaiser E. (2001) The nature of giant cell tumor of bone. J Cancer Res Clin Oncol, 127: 467-474.
21. Cowan RW, Singh G. (2013) Giant cell tumor of bone: a basic science perspective. Bone, 52: 238-246.

22. Salerno M, Avnet S, Alberghini M, Giunti A, Baldini N. (2008) Histogenetic characterization of giant cell tumor of bone. Clin Orthop Relat Res, 466: 2081-2091.
23. Forsyth RG, Krenacs T, Athanasou N, Hogendoorn PCW. (2021) Cell Biology of Giant Cell Tumour of Bone: Crosstalk between m/wt Nucleosome H3.3, Telomeres and Osteoclastogenesis. Cancers (Basel), 13.
24. Moskovszky L, Szuhai K, Krenacs T, Hogendoorn PC, Szendroi M, Benassi MS, Kopper L, Fule T, Sapi Z. (2009) Genomic instability in giant cell tumor of bone. A study of 52 cases using DNA ploidy, relocalization FISH, and array-CGH analysis. Genes Chromosomes Cancer, 48: 468-479.
25. De Boeck G, Forsyth RG, Praet M, Hogendoorn PC. (2009) Telomere-associated proteins: cross-talk between telomere maintenance and telomere-lengthening mechanisms. The Journal of Pathology: A Journal of the Pathological Society of Great Britain and Ireland, 217: 327-344.
26. Forsyth RG, De Boeck G, Bekaert S, De Meyer T, Taminiau AH, Uyttendaele D, Roels H, Praet MM, Hogendoorn PC. (2008) Telomere biology in giant cell tumour of bone. J Pathol, 214: 555-563.
27. Presneau N, Baumhoer D, Behjati S, Pillay N, Tarpey P, Campbell PJ, Jundt G, Hamoudi R, Wedge DC, Loo PV, Hassan AB, Khatri B, Ye H, Tirabosco R, Amary MF, Flanagan AM. (2015) Diagnostic value of H3F3A mutations in giant cell tumour of bone compared to osteoclast-rich mimics. J Pathol Clin Res, 1: 113-123.
28. Amary F, Berisha F, Ye H, Gupta M, Gutteridge A, Baumhoer D, Gibbons R, Tirabosco R, O'Donnell P, Flanagan AM. (2017) H3F3A (Histone 3.3) G34W Immunohistochemistry: A Reliable Marker Defining Benign and Malignant Giant Cell Tumor of Bone. Am J Surg Pathol, 41: 1059-1068.
29. Fittall MW, Lyskjær I, Ellery P, Lombard P, Ijaz J, Strobl A-C, Oukrif D, Tarabichi M, Sill M, Koelsche C, Mechtersheimer G, Demeulemeester J, Tirabosco R, Amary F, Campbell PJ, Pfister SM, Jones DT, Pillay N, Van Loo P, Behjati S, Flanagan AM. (2020) Drivers underpinning the malignant transformation of giant cell tumour of bone. The Journal of Pathology, 252: 433-440.

30. Leske H, Dalgleish R, Lazar AJ, Reifenberger G, Cree IA. (2021) A common classification framework for histone sequence alterations in tumours: an expert consensus proposal. The Journal of Pathology, 254: 109-120.
31. Werner M. (2006) Giant cell tumour of bone: morphological, biological and histogenetical aspects. International Orthopaedics, 30: 484-489.
32. Ariizumi T, Ogose A, Kawashima H, Hotta T, Umezu H, Endo N. (2009) Multinucleation followed by an acytokinetic cell division in myxofibrosarcoma with giant cell proliferation. J Exp Clin Cancer Res, 28: 44.
33. Rieder CL, Maiato H. (2004) Stuck in Division or Passing through: What Happens When Cells Cannot Satisfy the Spindle Assembly Checkpoint. Developmental Cell, 7: 637-651.
34. Rengstl B, Newrzela S, Heinrich T, Weiser C, Thalheimer FB, Schmid F, Warner K, Hartmann S, Schroeder T, Küppers R, Rieger MA, Hansmann M-L. (2013) Incomplete cytokinesis and re-fusion of small mononucleated Hodgkin cells lead to giant multinucleated Reed–Sternberg cells. Proceedings of the National Academy of Sciences, 110: 20729-20734.
35. Vignery A. (2005) Macrophage fusion: the making of osteoclasts and giant cells. J Exp Med, 202: 337-340.
36. Herrtwich L, Nanda I, Evangelou K, Nikolova T, Horn V, Sagar, Erny D, Stefanowski J, Rogell L, Klein C, Gharun K, Follo M, Seidl M, Kremer B, Münke N, Senges J, Fliegauf M, Aschman T, Pfeifer D, Sarrazin S, Sieweke MH, Wagner D, Dierks C, Haaf T, Ness T, Zaiss MM, Voll RE, Deshmukh SD, Prinz M, Goldmann T, Hölscher C, Hauser AE, Lopez-Contreras AJ, Grün D, Gorgoulis V, Diefenbach A, Henneke P, Triantafyllopoulou A. (2016) DNA Damage Signaling Instructs Polyploid Macrophage Fate in Granulomas. Cell, 167: 1264-1280.e1218.
37. Choi JW, Lee JH, Kim YS. (2011) Frequent Upregulation of Cyclin D1 and p16INK4a Expression with Low Ki-67 Scores in Multinucleated Giant Cells. Pathobiology, 78: 233-237.
38. Yao Y, Cai X, Ren F, Ye Y, Wang F, Zheng C, Qian Y, Zhang M. (2021) The Macrophage-Osteoclast Axis in Osteoimmunity and Osteo-Related Diseases. Frontiers in Immunology, 12.

39. Kapellos TS, Bonaguro L, Gemünd I, Reusch N, Saglam A, Hinkley ER, Schultze JL. (2019) Human Monocyte Subsets and Phenotypes in Major Chronic Inflammatory Diseases. Frontiers in Immunology, 10.
40. Mantovani A, Sica A, Sozzani S, Allavena P, Vecchi A, Locati M. (2004) The chemokine system in diverse forms of macrophage activation and polarization. Trends in Immunology, 25: 677-686.
41. Sun Y, Li J, Xie X, Gu F, Sui Z, Zhang K, Yu T. (2021) Macrophage-Osteoclast Associations: Origin, Polarization, and Subgroups. Frontiers in Immunology, 12.
42. Brooks PJ, Glogauer M, McCulloch CA. (2019) An Overview of the Derivation and Function of Multinucleated Giant Cells and Their Role in Pathologic Processes. The American Journal of Pathology, 189: 1145-1158.
43. Knowles HJ, Athanasou NA. (2009) Acute hypoxia and osteoclast activity: a balance between enhanced resorption and increased apoptosis. The Journal of Pathology, 218: 256-264.
44. Knowles HJ, Athanasou NA. (2008) Hypoxia-inducible factor is expressed in giant cell tumour of bone and mediates paracrine effects of hypoxia on monocyte-osteoclast differentiation via induction of VEGF. J Pathol, 215: 56-66.
45. Maggiani F, Forsyth R, Hogendoorn PC, Krenacs T, Athanasou NA. (2011) The immunophenotype of osteoclasts and macrophage polykaryons. J Clin Pathol, 64: 701-705.
46. Kandel R, Li SQ, Bell R, Wunder J, Ferguson P, Kauzman A, Diehl JA, Werier J. (2006) Cyclin D1 and p21 is elevated in the giant cells of giant cell tumors. J Orthop Res, 24: 428-437.
47. Kauzman A, Li SQ, Bradley G, Bell RS, Wunder JS, Kandel R. (2003) Cyclin alterations in giant cell tumor of bone. Mod Pathol, 16: 210-218.
48. Matsubayashi S, Nakashima M, Kumagai K, Egashira M, Naruke Y, Kondo H, Hayashi T, Shindo H. (2009) Immunohistochemical analyses of beta-catenin and cyclin D1 expression in giant cell tumor of bone (GCTB): a possible role of Wnt pathway in GCTB tumorigenesis. Pathol Res Pract, 205: 626-633.
49. Tachibana KE, Gonzalez MA, Coleman N. (2005) Cell-cycle-dependent regulation of DNA replication and its relevance to cancer pathology. J Pathol, 205: 123-129.

50. Williams GH, Stoeber K. (2007) Cell cycle markers in clinical oncology. Curr Opin Cell Biol, 19: 672-679.
51. Williams GH, Stoeber K. (2012) The cell cycle and cancer. J Pathol, 226: 352-364.
52. Kingsbury SR, Loddo M, Fanshawe T, Obermann EC, Prevost AT, Stoeber K, Williams GH. (2005) Repression of DNA replication licensing in quiescence is independent of geminin and may define the cell cycle state of progenitor cells. Exp Cell Res, 309: 56-67.
53. Marescal O, Cheeseman IM. (2020) Cellular Mechanisms and Regulation of Quiescence. Developmental Cell, 55: 259-271.
54. Terzi MY, Izmirli M, Gogebakan B. (2016) The cell fate: senescence or quiescence. Molecular Biology Reports, 43: 1213-1220.
55. Zetterberg A, Larsson O. (1985) Kinetic analysis of regulatory events in G1 leading to proliferation or quiescence of Swiss 3T3 cells. Proc Natl Acad Sci U S A, 82: 5365-5369.
56. Planas-Silva MD, Weinberg RA. (1997) The restriction point and control of cell proliferation. Curr Opin Cell Biol, 9: 768-772.
57. Gonzalez MA, Tachibana KE, Laskey RA, Coleman N. (2005) Control of DNA replication and its potential clinical exploitation. Nat Rev Cancer, 5: 135-141.
58. Vijayraghavan S, Schwacha A. (2012) The eukaryotic Mcm2-7 replicative helicase. Subcell Biochem, 62: 113-134.
59. Loddo M, Kingsbury SR, Rashid M, Proctor I, Holt C, Young J, El-Sheikh S, Falzon M, Eward KL, Prevost T, Sainsbury R, Stoeber K, Williams GH. (2009) Cell-cycle-phase progression analysis identifies unique phenotypes of major prognostic and predictive significance in breast cancer. Br J Cancer, 100: 959-970.
60. Orford KW, Scadden DT. (2008) Deconstructing stem cell self-renewal: genetic insights into cell-cycle regulation. Nat Rev Genet, 9: 115-128.
61. Sherr CJ. (1995) D-type cyclins. Trends Biochem Sci, 20: 187-190.
62. Lapenna S, Giordano A. (2009) Cell cycle kinases as therapeutic targets for cancer. Nature Reviews Drug Discovery, 8: 547-566.

63. O'Leary B, Finn RS, Turner NC. (2016) Treating cancer with selective CDK4/6 inhibitors. Nature Reviews Clinical Oncology, 13: 417-430.
64. Bartek J, Lukas J, Bartkova J. (1999) Perspective: defects in cell cycle control and cancer. J Pathol, 187: 95-99.
65. Harbour JW, Luo RX, Dei Santi A, Postigo AA, Dean DC. (1999) Cdk phosphorylation triggers sequential intramolecular interactions that progressively block Rb functions as cells move through G1. Cell, 98: 859-869.
66. Malumbres M, Barbacid M. (2009) Cell cycle, CDKs and cancer: a changing paradigm. Nature Reviews Cancer, 9: 153-166.
67. Carnero A, Hannon GJ. (1998) The INK4 family of CDK inhibitors. Curr Top Microbiol Immunol, 227: 43-55.
68. Arellano M, Moreno S. (1997) Regulation of CDK/cyclin complexes during the cell cycle. Int J Biochem Cell Biol, 29: 559-573.
69. Vermeulen K, Van Bockstaele DR, Berneman ZN. (2003) The cell cycle: a review of regulation, deregulation and therapeutic targets in cancer. Cell Proliferation, 36: 131-149.
70. Villman K, Stahl E, Liljegren G, Tidefelt U, Karlsson MG. (2002) Topoisomerase II-alpha expression in different cell cycle phases in fresh human breast carcinomas. Mod Pathol, 15: 486-491.
71. Kiszner G, Wichmann B, Nemeth IB, Varga E, Meggyeshazi N, Teleki I, Balla P, Maros ME, Penksza K, Krenacs T. (2014) Cell cycle analysis can differentiate thin melanomas from dysplastic nevi and reveals accelerated replication in thick melanomas. Virchows Arch, 464: 603-612.
72. Murray AW. (2004) Recycling the cell cycle: cyclins revisited. Cell, 116: 221-234.
73. Shetty A, Loddo M, Fanshawe T, Prevost AT, Sainsbury R, Williams GH, Stoeber K. (2005) DNA replication licensing and cell cycle kinetics of normal and neoplastic breast. Br J Cancer, 93: 1295-1300.
74. Xouri G, Dimaki M, Bastiaens PI, Lygerou Z. (2007) Cdt1 interactions in the licensing process: a model for dynamic spatiotemporal control of licensing. Cell Cycle, 6: 1549-1552.

75. Xouri G, Squire A, Dimaki M, Geverts B, Verveer PJ, Taraviras S, Nishitani H, Houtsmuller AB, Bastiaens PI, Lygerou Z. (2007) Cdt1 associates dynamically with chromatin throughout G1 and recruits Geminin onto chromatin. EMBO J, 26: 1303-1314.
76. Scott IS, Morris LS, Bird K, Davies RJ, Vowler SL, Rushbrook SM, Marshall AE, Laskey RA, Miller R, Arends MJ, Coleman N. (2003) A novel immunohistochemical method to estimate cell-cycle phase distribution in archival tissue: implications for the prediction of outcome in colorectal cancer. J Pathol, 201: 187-197.
77. Hightower E, Cabanillas ME, Fuller GN, McCutcheon IE, Hess KR, Shah K, Waguespack SG, Corley LJ, Devin JK. (2012) Phospho-histone H3 (pHH3) immuno-reactivity as a prognostic marker in non-functioning pituitary adenomas. Pituitary, 15: 556-561.
78. Gerlach U, Kayser G, Walch A, Hopt U, Schulte-Mönting J, Werner M, Lassmann S. (2006) Centrosome-, chromosomal-passenger- and cell-cycle-associated mRNAs are differentially regulated in the development of sporadic colorectal cancer. The Journal of Pathology, 208: 462-472.
79. Lacroix B, Maddox AS. (2012) Cytokinesis, ploidy and aneuploidy. J Pathol, 226: 338-351.
80. Vindelov LL, Christensen IJ. (1990) A review of techniques and results obtained in one laboratory by an integrated system of methods designed for routine clinical flow cytometric DNA analysis. Cytometry, 11: 753-770.
81. Engelholm SA, Spang-Thomsen M, Vindelov LL, Brunner NA. (1986) Chemosensitivity of human small cell carcinoma of the lung detected by flow cytometric DNA analysis of drug-induced cell cycle perturbations in vitro. Cytometry, 7: 243-250.
82. Nunez R. (2001) DNA measurement and cell cycle analysis by flow cytometry. Curr Issues Mol Biol, 3: 67-70.
83. Ganem NJ, Pellman D. (2007) Limiting the proliferation of polyploid cells. Cell, 131: 437-440.
84. Kimura SH, Nojima H. (2002) Cyclin G1 associates with MDM2 and regulates accumulation and degradation of p53 protein. Genes to Cells, 7: 869-880.

85. Moll UM, Petrenko O. (2003) The MDM2-p53 Interaction. Molecular Cancer Research, 1: 1001-1008.
86. Okamoto K, Li H, Jensen MR, Zhang T, Taya Y, Thorgeirsson SS, Prives C. (2002) Cyclin G Recruits PP2A to Dephosphorylate Mdm2. Molecular Cell, 9: 761-771.
87. Gordon EM, Ravicz JR, Liu S, Chawla SP, Hall FL. (2018) Cell cycle checkpoint control: The cyclin G1/Mdm2/p53 axis emerges as a strategic target for broad-spectrum cancer gene therapy - A review of molecular mechanisms for oncologists. Mol Clin Oncol, 9: 115-134.
88. Hanna-Morris A, Badvie S, Cohen P, McCullough T, Andreyev HJ, Allen-Mersh TG. (2009) Minichromosome maintenance protein 2 (MCM2) is a stronger discriminator of increased proliferation in mucosa adjacent to colorectal cancer than Ki-67. J Clin Pathol, 62: 325-330.
89. Papay J, Krenacs T, Moldvay J, Stelkovics E, Furak J, Molnar B, Kopper L. (2007) Immunophenotypic profiling of nonsmall cell lung cancer progression using the tissue microarray approach. Appl Immunohistochem Mol Morphol, 15: 19-30.
90. Lopez-Guerrero JA, Machado I, Scotlandi K, Noguera R, Pellin A, Navarro S, Serra M, Calabuig-Farinas S, Picci P, Llombart-Bosch A. (2011) Clinicopathological significance of cell cycle regulation markers in a large series of genetically confirmed Ewing's sarcoma family of tumors. Int J Cancer, 128: 1139-1150.
91. Lujic N, Sopta J, Kovacevic R, Stevanovic V, Davidovic R. (2016) Recurrence of giant cell tumour of bone: role of p53, cyclin D1, β-catenin and Ki67. International Orthopaedics, 40: 2393-2399.
92. Maros ME, Schnaidt S, Balla P, Kelemen Z, Sapi Z, Szendroi M, Laszlo T, Forsyth R, Picci P, Krenacs T. (2019) In situ cell cycle analysis in giant cell tumor of bone reveals patients with elevated risk of reduced progression-free survival. Bone, 127: 188-198.
93. Pazzaglia L, Benassi MS, Ragazzini P, Gamberi G, Ponticelli F, Chiechi A, Hattinger CM, Morandi L, Alberghini M, Zanella L, Picci P, Mercuri M. (2006) Molecular alterations of monophasic synovial sarcoma: loss of chromosome 3p

does not alter RASSF1 and MLH1 transcriptional activity. Histol Histopathol, 21: 187-195.

94. Prentice RL, Williams BJ, Peterson AV. (1981) On the Regression-Analysis of Multivariate Failure Time Data. Biometrika, 68: 373-379.

95. Prentice RL. (1985) Relative risk regression analysis of epidemiologic data. Environ Health Perspect, 63: 225-234.

96. Yang W, Jepson C, Xie D, Roy JA, Shou H, Hsu JY, Anderson AH, Landis JR, He J, Feldman HI. (2017) Statistical Methods for Recurrent Event Analysis in Cohort Studies of CKD. Clinical Journal of the American Society of Nephrology, 12: 2066.

97. Amorim LDAF, Cai J. (2015) Modelling recurrent events: a tutorial for analysis in epidemiology. International Journal of Epidemiology, 44: 324-333.

98. Vittinghoff E, McCulloch CE. (2007) Relaxing the rule of ten events per variable in logistic and Cox regression. Am J Epidemiol, 165: 710-718.

99. van Houwelingen HC. (2014) From model building to validation and back: a plea for robustness. Stat Med, 33: 5223-5238.

100. Bradburn M, Clark T, Love S, Altman D. (2003) Survival analysis Part III: multivariate data analysis–choosing a model and assessing its adequacy and fit. British journal of cancer, 89: 605-611.

101. Enneking WF. (1986) A system of staging musculoskeletal neoplasms. Clin Orthop Relat Res: 9-24.

102. Campanacci M, Baldini N, Boriani S, Sudanese A. (1987) Giant-cell tumor of bone. The Journal of bone and joint surgery. American volume, 69: 106-114.

103. Amelio JM, Rockberg J, Hernandez RK, Sobocki P, Stryker S, Bach BA, Engellau J, Liede A. (2016) Population-based study of giant cell tumor of bone in Sweden (1983–2011). Cancer Epidemiology, 42: 82-89.

104. Palmerini E, Seeger LL, Gambarotti M, Righi A, Reichardt P, Bukata S, Blay J-Y, Dai T, Jandial D, Picci P. (2021) Malignancy in giant cell tumor of bone: analysis of an open-label phase 2 study of denosumab. BMC Cancer, 21: 89.

105. Chawla S, Blay J-Y, Rutkowski P, Le Cesne A, Reichardt P, Gelderblom H, Grimer RJ, Choy E, Skubitz K, Seeger L, Schuetze SM, Henshaw R, Dai T, Jandial D, Palmerini E. (2019) Denosumab in patients with giant-cell tumour of

bone: a multicentre, open-label, phase 2 study. The Lancet Oncology, 20: 1719-1729.

106. Nascimento AG, Huvos AG, Marcove RC. (1979) Primary malignant giant cell tumor of bone: a study of eight cases and review of the literature. Cancer, 44: 1393-1402.

107. Gong L, Liu W, Sun X, Sajdik C, Tian X, Niu X, Huang X. (2012) Histological and clinical characteristics of malignant giant cell tumor of bone. Virchows Archiv, 460: 327-334.

108. Wojcik J, Rosenberg AE, Bredella MA, Choy E, Hornicek FJ, Nielsen GP, Deshpande V. (2016) Denosumab-treated Giant Cell Tumor of Bone Exhibits Morphologic Overlap With Malignant Giant Cell Tumor of Bone. Am J Surg Pathol, 40: 72-80.

109. van der Heijden L, Dijkstra PDS, Blay J-Y, Gelderblom H. (2017) Giant cell tumour of bone in the denosumab era. European Journal of Cancer, 77: 75-83.

110. Szendrői M. Giant-cell tumour of bone (GCT). In: European Surgical Orthopaedics and Traumatology. Springer, 2014: 4037-4054.

111. Rockberg J, Bach BA, Amelio J, Hernandez RK, Sobocki P, Engellau J, Bauer HC, Liede A. (2015) Incidence Trends in the Diagnosis of Giant Cell Tumor of Bone in Sweden Since 1958. J Bone Joint Surg Am, 97: 1756-1766.

112. Klenke FM, Wenger DE, Inwards CY, Rose PS, Sim FH. (2011) Giant Cell Tumor of Bone: Risk Factors for Recurrence. Clinical Orthopaedics and Related Research®, 469.

113. Lee JC, Liang CW, Fletcher CD. (2017) Giant cell tumor of soft tissue is genetically distinct from its bone counterpart. Mod Pathol, 30: 728-733.

114. Lim J, Park JH, Baude A, Yoo Y, Lee YK, Schmidt CR, Park JB, Fellenberg J, Zustin J, Haller F, Krücken I, Kang HG, Park YJ, Plass C, Lindroth AM. (2017) The histone variant H3.3 G34W substitution in giant cell tumor of the bone link chromatin and RNA processing. Scientific Reports, 7: 13459.

115. Venneker S, van Eenige R, Kruisselbrink AB, Palubeckaitė I, Taliento AE, Briaire-de Bruijn IH, Hogendoorn PCW, van de Sande MAJ, Gelderblom H, Mei H, Bovée JVMG, Szuhai K. (2022) Histone Deacetylase Inhibitors as a

Therapeutic Strategy to Eliminate Neoplastic "Stromal" Cells from Giant Cell Tumors of Bone. Cancers, 14: 4708.

116. Yamamoto H, Ishihara S, Toda Y, Oda Y. (2020) Histone H3.3 mutation in giant cell tumor of bone: an update in pathology. Medical Molecular Morphology, 53: 1-6.
117. Malumbres M, Sotillo R, Santamaria D, Galan J, Cerezo A, Ortega S, Dubus P, Barbacid M. (2004) Mammalian cells cycle without the D-type cyclin-dependent kinases Cdk4 and Cdk6. Cell, 118: 493-504.
118. Spring LM, Wander SA, Andre F, Moy B, Turner NC, Bardia A. (2020) Cyclin-dependent kinase 4 and 6 inhibitors for hormone receptor-positive breast cancer: past, present, and future. The Lancet, 395: 817-827.
119. Finn RS, Aleshin A, Slamon DJ. (2016) Targeting the cyclin-dependent kinases (CDK) 4/6 in estrogen receptor-positive breast cancers. Breast Cancer Research, 18: 17.
120. Shapiro GI. (2017) Genomic Biomarkers Predicting Response to Selective CDK4/6 Inhibition: Progress in an Elusive Search. Cancer Cell, 32: 721-723.
121. Wander SA, Cohen O, Gong X, Johnson GN, Buendia-Buendia JE, Lloyd MR, Kim D, Luo F, Mao P, Helvie K, Kowalski KJ, Nayar U, Waks AG, Parsons SH, Martinez R, Litchfield LM, Ye XS, Yu C, Jansen VM, Stille JR, Smith PS, Oakley GJ, Chu QS, Batist G, Hughes ME, Kremer JD, Garraway LA, Winer EP, Tolaney SM, Lin NU, Buchanan SG, Wagle N. (2020) The Genomic Landscape of Intrinsic and Acquired Resistance to Cyclin-Dependent Kinase 4/6 Inhibitors in Patients with Hormone Receptor–Positive Metastatic Breast Cancer. Cancer Discovery, 10: 1174-1193.
122. Joshi S, Watkins J, Gazinska P, Brown JP, Gillett CE, Grigoriadis A, Pinder SE. (2015) Digital imaging in the immunohistochemical evaluation of the proliferation markers Ki67, MCM2 and Geminin, in early breast cancer, and their putative prognostic value. BMC Cancer, 15: 546.
123. Matsumoto Y, Maller JL. (2004) A Centrosomal Localization Signal in Cyclin E Required for Cdk2-Independent S Phase Entry. Science, 306: 885-888.

124. De Boer L, Oakes V, Beamish H, Giles N, Stevens F, Somodevilla-Torres M, DeSouza C, Gabrielli B. (2008) Cyclin A/cdk2 coordinates centrosomal and nuclear mitotic events. Oncogene, 27: 4261-4268.
125. Molendini L, Benassi MS, Magagnoli G, Merli M, Sollazzo MR, Ragazzini P, Gamberi G, Ferrari C, Balladelli A, Bacchini P, Picci P. (1998) Prognostic significance of cyclin expression in human osteosarcoma. Int J Oncol, 12: 1007-1011.
126. Yoshida K, Oyaizu N, Dutta A, Inoue I. (2004) The destruction box of human Geminin is critical for proliferation and tumor growth in human colon cancer cells. Oncogene, 23: 58-70.
127. Shrestha P, Saito T, Hama S, Arifin MT, Kajiwara Y, Yamasaki F, Hidaka T, Sugiyama K, Kurisu K. (2007) Geminin: A good prognostic factor in high-grade astrocytic brain tumors. Cancer, 109: 949-956.
128. Wharton SB, Hibberd S, Eward KL, Crimmins D, Jellinek DA, Levy D, Stoeber K, Williams GH. (2004) DNA replication licensing and cell cycle kinetics of oligodendroglial tumours. Br J Cancer, 91: 262-269.
129. Xu L, Jin J, Hu A, Xiong J, Wang D, Sun Q, Wang S. (2017) Soft tissue recurrence of giant cell tumor of the bone: Prevalence and radiographic features. Journal of Bone Oncology, 9: 10-14.
130. Li D, Zhang J, Li Y, Xia J, Yang Y, Ren M, Liao Y, Yu S, Li X, Shen Y, Zhang Y, Yang Z. (2016) Surgery methods and soft tissue extension are the potential risk factors of local recurrence in giant cell tumor of bone. World Journal of Surgical Oncology, 14: 114.
131. Steyerberg EW, Borsboom GJ, van Houwelingen HC, Eijkemans MJ, Habbema JD. (2004) Validation and updating of predictive logistic regression models: a study on sample size and shrinkage. Stat Med, 23: 2567-2586.
132. Harrell FE, Jr., Lee KL, Mark DB. (1996) Multivariable prognostic models: issues in developing models, evaluating assumptions and adequacy, and measuring and reducing errors. Stat Med, 15: 361-387.
133. Steyerberg EW, Eijkemans MJ, Harrell FE, Jr., Habbema JD. (2001) Prognostic modeling with logistic regression analysis: in search of a sensible strategy in small data sets. Med Decis Making, 21: 45-56.

134. Steyerberg EW, Harrell FE, Jr. (2016) Prediction models need appropriate internal, internal-external, and external validation. J Clin Epidemiol, 69: 245-247.
135. Steyerberg EW, Schemper M, Harrell FE. (2011) Logistic regression modeling and the number of events per variable: selection bias dominates. J Clin Epidemiol, 64: 1464-1465; author reply 1463-1464.
136. Steyerberg EW, Vergouwe Y. (2014) Towards better clinical prediction models: seven steps for development and an ABCD for validation. Eur Heart J, 35: 1925-1931.
137. Li H, Gao J, Gao Y, Lin N, Zheng M, Ye Z. (2020) Denosumab in Giant Cell Tumor of Bone: Current Status and Pitfalls. Frontiers in Oncology, 10.
138. Gaston CL, Grimer RJ, Parry M, Stacchiotti S, Dei Tos AP, Gelderblom H, Ferrari S, Baldi GG, Jones RL, Chawla S, Casali P, LeCesne A, Blay JY, Dijkstra SP, Thomas DM, Rutkowski P. (2016) Current status and unanswered questions on the use of Denosumab in giant cell tumor of bone. Clin Sarcoma Res, 6: 15.
139. Antal I, Pápai Z, Szendrői M, Perlaky T, Dezső K, Lippai Z, Sápi Z. (2022) The Activation of PDGFRβ on Mononuclear Stromal/Tumor Cells in Giant Cell Tumor of Bone After Denosumab Treatment. An Immunohistochemical Study of Five Cases. Pathology and Oncology Research, 28.
140. Mahdal M, Neradil J, Mudry P, Paukovcekova S, Staniczkova Zambo I, Urban J, Macsek P, Pazourek L, Tomas T, Veselska R. New Target for Precision Medicine Treatment of Giant-Cell Tumor of Bone: Sunitinib Is Effective in the Treatment of Neoplastic Stromal Cells with Activated PDGFRβ Signaling. In: Cancers Vol. 13, 2021.
141. Sanchez-Pareja A, Larousserie F, Boudabbous S, Beaulieu JY, Mach N, Saiji E, Rougemont AL. (2016) Giant Cell Tumor of Bone With Pseudosarcomatous Changes Leading to Premature Denosumab Therapy Interruption: A Case Report With Review of the Literature. Int J Surg Pathol, 24: 366-372.
142. Sun X, Kaufman PD. (2018) Ki-67: more than a proliferation marker. Chromosoma, 127: 175-186.
143. Sales Gil R, Vagnarelli P. (2018) Ki-67: More Hidden behind a 'Classic Proliferation Marker'. Trends in Biochemical Sciences, 43: 747-748.

144. Miller I, Min M, Yang C, Tian C, Gookin S, Carter D, Spencer SL. (2018) Ki67 is a Graded Rather than a Binary Marker of Proliferation versus Quiescence. Cell Reports, 24: 1105-1112.e1105.
145. Sobecki M, Mrouj K, Camasses A, Parisis N, Nicolas E, Llères D, Gerbe F, Prieto S, Krasinska L, David A, Eguren M, Birling M-C, Urbach S, Hem S, Déjardin J, Malumbres M, Jay P, Dulic V, Lafontaine DLJ, Feil R, Fisher D. (2016) The cell proliferation antigen Ki-67 organises heterochromatin. eLife, 5: e13722.
146. Ismail FW, Shamsudin AM, Wan Z, Daud SM, Samarendra MS. (2010) Ki-67 immuno-histochemistry index in stage III giant cell tumor of the bone. Journal of Experimental & Clinical Cancer Research, 29: 25.
147. Lindboe CF, Torp SH. (2002) Comparison of Ki-67 equivalent antibodies. J Clin Pathol, 55: 467-471.
148. Vijayraghavan S, Schwacha A. The Eukaryotic Mcm2-7 Replicative Helicase. In: MacNeill S (szerk.), The Eukaryotic Replisome: a Guide to Protein Structure and Function, doi:10.1007/978-94-007-4572-8_7. Springer Netherlands, Dordrecht, 2012: 113-134.
149. Pestell RG. (2013) New Roles of Cyclin D1. The American Journal of Pathology, 183: 3-9.
150. Sherr CJ, Roberts JM. (2004) Living with or without cyclins and cyclin-dependent kinases. Genes Dev, 18: 2699-2711.
151. Geng Y, Lee Y-M, Welcker M, Swanger J, Zagozdzon A, Winer JD, Roberts JM, Kaldis P, Clurman BE, Sicinski P. (2007) Kinase-independent function of cyclin E. Molecular cell, 25: 127-139.
152. Loeb KR, Kostner H, Firpo E, Norwood T, D. Tsuchiya K, Clurman BE, Roberts JM. (2005) A mouse model for cyclin E-dependent genetic instability and tumorigenesis. Cancer Cell, 8: 35-47.
153. Olvera M, Harris S, Amezcua CA, McCourty A, Rezk S, Koo C, Felix JC, Brynes RK. (2001) Immunohistochemical expression of cell cycle proteins E2F-1, Cdk-2, Cyclin E, p27(kip1), and Ki-67 in normal placenta and gestational trophoblastic disease. Mod Pathol, 14: 1036-1042.

154. Romero-Pozuelo J, Figlia G, Kaya O, Martin-Villalba A, Teleman AA. (2020) Cdk4 and Cdk6 Couple the Cell-Cycle Machinery to Cell Growth via mTORC1. Cell Reports, 31: 107504.
155. Fu M, Wang C, Li Z, Sakamaki T, Pestell RG. (2004) Minireview: Cyclin D1: normal and abnormal functions. Endocrinology, 145: 5439-5447.
156. Planas-Silva MD, Weinberg RA. (1997) Estrogen-dependent cyclin E-cdk2 activation through p21 redistribution. Mol Cell Biol, 17: 4059-4069.
157. Soonpaa MH, Koh GY, Pajak L, Jing S, Wang H, Franklin MT, Kim KK, Field LJ. (1997) Cyclin D1 overexpression promotes cardiomyocyte DNA synthesis and multinucleation in transgenic mice. J Clin Invest, 99: 2644-2654.
158. Palazon LS, Davies TJ, Gardner RL. (1998) Translational inhibition of cyclin B1 and appearance of cyclin D1 very early in the differentiation of mouse trophoblast giant cells. Mol Hum Reprod, 4: 1013-1020.
159. Georgakilas AG, Martin OA, Bonner WM. (2017) p21: A Two-Faced Genome Guardian. Trends Mol Med, 23: 310-319.
160. Hafner A, Bulyk ML, Jambhekar A, Lahav G. (2019) The multiple mechanisms that regulate p53 activity and cell fate. Nature Reviews Molecular Cell Biology, 20: 199-210.
161. Gire V, Dulić V. (2015) Senescence from G2 arrest, revisited. Cell Cycle, 14: 297-304.
162. Cheng M, Olivier P, Diehl JA, Fero M, Roussel MF, Roberts JM, Sherr CJ. (1999) The p21(Cip1) and p27(Kip1) CDK 'inhibitors' are essential activators of cyclin D-dependent kinases in murine fibroblasts. Embo j, 18: 1571-1583.
163. Alt JR, Cleveland JL, Hannink M, Diehl JA. (2000) Phosphorylation-dependent regulation of cyclin D1 nuclear export and cyclin D1-dependent cellular transformation. Genes Dev, 14: 3102-3114.
164. Alt JR, Gladden AB, Diehl JA. (2002) p21(Cip1) Promotes cyclin D1 nuclear accumulation via direct inhibition of nuclear export. J Biol Chem, 277: 8517-8523.
165. Mao Z, Ke Z, Gorbunova V, Seluanov A. (2012) Replicatively senescent cells are arrested in G1 and G2 phases. Aging, 4: 431-435.

166. Sankar U, Patel K, Rosol TJ, Ostrowski MC. (2004) RANKL Coordinates Cell Cycle Withdrawal and Differentiation in Osteoclasts Through the Cyclin-Dependent Kinase Inhibitors p27KIP1 and p21CIP1. Journal of Bone and Mineral Research, 19: 1339-1348.
167. Sherr CJ, Roberts JM. (1999) CDK inhibitors: positive and negative regulators of G1-phase progression. Genes Dev, 13: 1501-1512.
168. Sherr CJ, Roberts JM. (1995) Inhibitors of mammalian G1 cyclin-dependent kinases. Genes Dev, 9: 1149-1163.
169. Alcorta DA, Xiong Y, Phelps D, Hannon G, Beach D, Barrett JC. (1996) Involvement of the cyclin-dependent kinase inhibitor p16 (INK4a) in replicative senescence of normal human fibroblasts. Proceedings of the National Academy of Sciences, 93: 13742-13747.
170. Coppé J-P, Rodier F, Patil CK, Freund A, Desprez P-Y, Campisi J. (2011) Tumor Suppressor and Aging Biomarker p16INK4a Induces Cellular Senescence without the Associated Inflammatory Secretory Phenotype*. Journal of Biological Chemistry, 286: 36396-36403.
171. Stepanova L, Leng X, Parker SB, Harper JW. (1996) Mammalian p50Cdc37 is a protein kinase-targeting subunit of Hsp90 that binds and stabilizes Cdk4. Genes & development, 10: 1491-1502.
172. Lindeman JHN, Hanemaaijer R, Mulder A, Dijkstra PDS, Szuhai K, Bromme D, Verheijen JH, Hogendoorn PCW. (2004) Cathepsin K Is the Principal Protease in Giant Cell Tumor of Bone. The American Journal of Pathology, 165: 593-600.
173. Kumta SM, Huang L, Cheng YY, Chow LTC, Lee KM, Zheng MH. (2003) Expression of VEGF and MMP-9 in giant cell tumor of bone and other osteolytic lesions. Life Sciences, 73: 1427-1436.
174. Ueda Y, Imai K, Tsuchiya H, Fujimoto N, Nakanishi I, Katsuda S, Seiki M, Okada Y. (1996) Matrix metalloproteinase 9 (gelatinase B) is expressed in multinucleated giant cells of human giant cell tumor of bone and is associated with vascular invasion. Am J Pathol, 148: 611-622.
175. Dimri GP, Hara E, Campisi J. (1994) Regulation of two E2F-related genes in presenescent and senescent human fibroblasts. Journal of Biological Chemistry, 269: 16180-16186.

176. Yalcinkaya U, Ugras N, Kabul S, Ocakoglu G, Bilgen MS. (2015) Prognostic value of p53 protein expression in giant cell tumor of bone. Pol J Pathol, 66: 389-396.
177. Papanastassiou I, Ioannou M, Papagelopoulos PJ, Arealis G, Mihas C, Iakovidou I, Demertzis N. (2010) P53 expression as a prognostic marker in giant cell tumor of bone: a pilot study. Orthopedics, 33.
178. Vassilev LT, Vu BT, Graves B, Carvajal D, Podlaski F, Filipovic Z, Kong N, Kammlott U, Lukacs C, Klein C, Fotouhi N, Liu EA. (2004) In Vivo Activation of the p53 Pathway by Small-Molecule Antagonists of MDM2. Science, 303: 844-848.
179. Nag S, Qin J, Srivenugopal KS, Wang M, Zhang R. (2013) The MDM2-p53 pathway revisited. J Biomed Res, 27: 254-271.
180. Orriss IR, Arnett TR. (2012) Rodent osteoclast cultures. Methods Mol Biol, 816: 103-117.

9. Bibliography of the publications relevant to the dissertation

1. **Maros ME**, Balla P, Micsik T, Sapi Z, Szendroi M, Groden C, Wenz H, Forsyth RG, Picci P, Krenacs T. Cell Cycle Regulatory Protein Expression in Multinucleated Giant Cells of Giant Cell Tumor of Bone: do They Proliferate? Pathology and Oncology Research. 2021;27(94). IF: 2.874.

2. **Maros ME**, Schnaidt S, Balla P, Kelemen Z, Sapi Z, Szendroi M, Laszlo T, Forsyth R, Picci P, Krenacs T. In situ cell cycle analysis in giant cell tumor of bone reveals patients with elevated risk of reduced progression-free survival. Bone. 2019;127:188-98. IF: 4.147.

3. Balla P, **Maros ME**, Barna G, Antal I, Papp G, Sapi Z, Athanasou NA, Benassi MS, Picci P, Krenacs T. Prognostic impact of reduced connexin43 expression and gap junction coupling of neoplastic stromal cells in giant cell tumor of bone. PLoS One. 2015;10(5):e0125316. IF: 3.057.

Impact factors as first author relevant to the dissertation: 7.021.
Impact factors as coauthor relevant to the dissertation: 3.057.
Sum of impact factors relevant to the dissertation: 10.078.

9.1 Bibliography of the publications not directly related to the dissertation

1. Szekely T, Wichmann B, **Maros ME**, Csizmadia A, Bodor C, Timar B, Krenacs T. (2022) Myelofibrosis progression grading based on type-I and type-III collagen and fibrillin-1 expression boosted by whole slide image analysis. Histopathology, doi:10.1111/his.14846. IF: 7.778.

2. Leinert JL, Weis M, **Maros ME**, Flachsenhaar C, Kosubek M, Durken M. (2022) Scurvy in a Supposedly Healthy 4-Year-Old Picky Eater with Leg Pain and Refusal to Walk. Klin Padiatr, doi:10.1055/a-1931-3876. IF: 1.236.

3. Centner F-S, Oster ME, Dally F-J, Sauter-Servaes J, Pelzer T, Schoettler JJ, Hahn B, Fairley A-M, Abdulazim A, Hackenberg KAM, Groden C, Etminan N, Krebs J, Thiel M, Wenz H, **Maros ME**. (2022) Comparative Analyses of the Impact of Different Criteria for Sepsis Diagnosis on Outcome in Patients with Spontaneous Subarachnoid Hemorrhage. Journal of Clinical Medicine, 11: 3873. IF: 4.964.

4. Kim HE, **Maros ME**, Siegel F, Ganslandt T. Rapid Convolutional Neural Networks for Gram-Stained Image Classification at Inference Time on Mobile Devices: Empirical Study from Transfer Learning to Optimization. In: Biomedicines Vol. 10, 2022. IF: 4.757.

5. Weyer V, **Maros ME**, Kirschner S, Krost-Reuhl S, Groden C, Kramer M, Brockmann MA, Kronfeld A. (2022) Influence of neurovascular anatomy on perforation site in different mouse strains using the filament perforation model for induction of subarachnoid hemorrhage. PLoS One, 17: e0263983. IF: 3.752.

6. Kim HE, Cosa-Linan A, Santhanam N, Jannesari M, **Maros ME***, Ganslandt T*. Transfer learning for medical image classification: a literature review. BMC Med Imaging. 2022;22(1):69. IF: 2.795. *contributed equally.

7. Szekely T, Krenacs T, **Maros ME**, Bodor C, Daubner V, Csizmadia A, Vrabely B and Timar B. Correlations Between the Expression of Stromal Cell Activation Related Biomarkers, L-NGFR, Phospho-ERK1-2 and CXCL12, and Primary Myelofibrosis Progression. Pathology and Oncology Research. 2022;28(16):102-17. IF: 2.874.

8. Kampgen B, Sodmann PF, **Maros ME**, Kluter A. Verstehen was Ärzte schreiben: Kann KI die Datenflut in der Medizin bändigen? (25. fejezet). In: Pfannstiel, M.A. (szerk.) Künstliche Intelligenz im Gesundheitswesen. Springer Gabler, Wiesbaden, 2022:547-564. ISBN 978 3 658 33596 0.

9. Baazaoui H, Hubertus S, **Maros ME**, Mohamed SA, Förster A, Schad LR, et al. Artificial Neural Network-Derived Cerebral Metabolic Rate of Oxygen for Differentiating Glioblastoma and Brain Metastasis in MRI: A Feasibility Study. Applied Sciences. 2021;11(21):9928. IF: 2.838.

10. **Maros ME**, Brekenfeld C, Broocks G, Leischner H, McDonough R, Deb-Chatterji M, Alegiani A, Thomalla G, Fiehler J, Flottmann F, Investigators* GSR. Number of Retrieval Attempts Rather Than Procedure Time Is Associated With Risk of Symptomatic Intracranial Hemorrhage. Stroke. 2021;52(5):1580-8. IF: 10.170.

11. **Maros ME**, Cho CG, Junge AG, Kampgen B, Saase V, Siegel F, Trinkmann F, Ganslandt T, Groden C, Wenz H. Comparative analysis of machine learning algorithms for computer-assisted reporting based on fully automated cross-lingual RadLex mappings. Sci Rep. 2021;11(1):5529. IF: 4.997.

12. Flottmann F, Brekenfeld C, Broocks G, Leischner H, McDonough R, Faizy TD, Deb-Chatterji M, Alegiani A, Thomalla G, Mpotsaris A, Nolte CH, Fiehler J, **Maros ME**, investigators* GSR. Good Clinical Outcome Decreases With Number of Retrieval Attempts in Stroke Thrombectomy: Beyond the First-Pass Effect. Stroke. 2021;52(2):482-90. IF: 10.170.

13. Flottmann F, van Horn N, **Maros ME**, McDonough R, Deb-Chatterji M, Alegiani A, Thomalla G, Hanning U, Fiehler J, Brekenfeld C, investigators GSR. Early TICI 2b or Late TICI 3-Is Perfect the Enemy of Good? Clin Neuroradiol. 2021. IF: 3.156.

14. Flottmann F, van Horn N, **Maros ME**, Leischner H, Bechstein M, Meyer L, Sauer M, Deb-Chatterji M, Alegiani A, Thomalla G, Fiehler J, Brekenfeld C, investigators GSR. More Retrieval Attempts are Associated with Poorer Functional Outcome After Unsuccessful Thrombectomy. Clin Neuroradiol. 2021. IF: 3.156.

15. Trinkmann F, **Maros M**, Roth K, Hermanns A, Schafer J, Gawlitza J, Saur J, Akin I, Borggrefe M, Herth FJF, Ganslandt T. Multiple breath washout (MBW) testing using sulfur hexafluoride: reference values and influence of anthropometric parameters. Thorax. 2021;76(4):380-6. IF: 9.203.

16. Wichmann B, **Maros ME**, Fabian G, Szász AM. Biostasztika, bioinformatika: A biostatisztika patológiai alkalmazása (18. fejezet). In: Krenacs T, Bodor C, Matolcsy A (szerk.), Patológiai és molekuláris onkodiagnosztikai módszerek: Kézikönyv patológusoknak, kutatóknak, analitikusoknak, asszisztenseknek és a társszakmák képviselőinek. Medicina Könyvkiadó Zrt., Budapest, 2021:591-608. ISBN 978 963 226 767 8.

17. **Maros ME**, Capper D, Jones DTW, Hovestadt V, von Deimling A, Pfister SM, Benner A, Zucknick M, Sill M. Machine learning workflows to estimate class probabilities for precision cancer diagnostics on DNA methylation microarray data. Nat Protoc. 2020;15(2):479-512. IF: 13.491.

18. Westhoff N, Ritter M, **Maros M**, Rassweiler-Seyfried MC, Michel MS, Honeck P, von Hardenberg J. Prospective Feasibility Study of Single-Shot Antibiotic

Prophylaxis in Transrectal Focal Ablation of Prostate Cancer. Urol Int. 2020;104(5-6):378-85. IF: 2.089.

19. Weyer V*, **Maros ME***, Kronfeld A, Kirschner S, Groden C, Sommer C, Tanyildizi Y, Kramer M, Brockmann MA. Longitudinal imaging and evaluation of SAH-associated cerebral large artery vasospasm in mice using micro-CT and angiography. J Cereb Blood Flow Metab. 2020;40(11):2265-77. IF: 6.200. *contributed equally.

20. Forster A, Bohme J, **Maros ME**, Brehmer S, Seiz-Rosenhagen M, Hanggi D, Wenz F, Groden C, Pope WB, Giordano FA. Longitudinal MRI findings in patients with newly diagnosed glioblastoma after intraoperative radiotherapy. J Neuroradiol. 2020;47(2):166-73. IF: 3.447.

21. Pino-Lopez L, Wenz H, Bohme J, **Maros M**, Schlichtenbrede F, Groden C, Forster A. Contrast-enhanced fat-suppressed FLAIR for the characterization of leptomeningeal inflammation in optic neuritis. Mult. Scler. J. 2019;25(6):792-800. IF: 5.412.

22. **Maros ME**, Wenz R, Forster A, Froelich MF, Groden C, Sommer WH, Schonberg SO, Henzler T, Wenz H. Objective Comparison Using Guideline-based Query of Conventional Radiological Reports and Structured Reports. In Vivo. 2018;32(4):843-9. IF: 1.609.

23. Forster A*, Wenz R*, **Maros ME***, Bohme J, Al-Zghloul M, Alonso A, Groden C, Wenz H. Anatomical distribution of cerebral microbleeds and intracerebral hemorrhage in vertebrobasilar dolichoectasia. PLoS One. 2018;13(4):e0196149. IF: 2.776. *contributed equally.

24. Al-Zghloul M, Wenz H, **Maros M**, Bohme J, Groden C, Forster A. Susceptibility Vessel Sign on T2*-Weighted Gradient Echo Imaging in Lacunar Infarction. In Vivo. 2018;32(4):973-6. IF: 1.609.

25. Wenz H, Wenz R, **Maros M**, Ehrlich G, Al-Zghloul M, Groden C, Forster A. Incidence, Locations, and Longitudinal Course of Cerebral Microbleeds in European Moyamoya. Stroke. 2017;48(2):307-13. IF: 6.239.

26. Gawlitza M, Bohme J, **Maros M**, Lobsien D, Michalski D, Groden C, Hoffmann KT, Forster A. FLAIR vascular hyperintensities and 4D MR angiograms for the estimation of collateral blood flow in anterior cerebral artery ischemia. PLoS One. 2017;12(2):e0172570. IF: 2.766.

27. Wenz H, Wenz R, **Maros ME**, Groden C, Schmieder K, Fontana J. The neglected need for psychological intervention in patients suffering from incidentally discovered intracranial aneurysms. Clin Neurol Neurosurg. 2016;143:65-70. IF: 1.381.

28. Wenz H, **Maros ME**, Meyer M, Gawlitza J, Forster A, Haubenreisser H, Kurth S, Schoenberg SO, Groden C, Henzler T. Intra-individual diagnostic image quality and organ-specific-radiation dose comparison between spiral cCT with iterative image reconstruction and z-axis automated tube current modulation and sequential cCT. Eur J Radiol Open. 2016;3:182-90. IF: NA.

29. Wenz H, **Maros ME**, Meyer M, Forster A, Haubenreisser H, Kurth S, Schoenberg SO, Flohr T, Leidecker C, Groden C, Scharf J, Henzler T. Image Quality of 3rd Generation Spiral Cranial Dual-Source CT in Combination with an Advanced Model Iterative Reconstruction Technique: A Prospective Intra-Individual Comparison Study to Standard Sequential Cranial CT Using Identical Radiation Dose. PLoS One. 2015;10(8):e0136054. IF: 3.057.

30. Wenz H, Kerl HU, **Maros ME**, Wenz R, Kalvin K, Groden C, Nolte I. Signal changes of the alar ligament in a healthy population: a dispositional or degenerative consequence? J Neurosurg-Spine. 2015;23(5):544-50. IF: 2.126.

31. Kirschner S, Felix MC, Hartmann L, Bierbaum M, **Maros ME**, Kerl HU, Wenz F, Glatting G, Kramer M, Giordano FA, Brockmann MA. In vivo micro-CT imaging of untreated and irradiated orthotopic glioblastoma xenografts in mice: capabilities, limitations and a comparison with bioluminescence imaging. J Neuro-oncol. 2015;122(2):245-54. IF: 2.754.

32. Andocs G, Meggyeshazi N, Balogh L, Spisak S, **Maros ME**, Balla P, Kiszner G, Teleki I, Kovago C, Krenacs T. Upregulation of heat shock proteins and the promotion of damage-associated molecular pattern signals in a colorectal cancer model by modulated electrohyperthermia. Cell Stress Chaperones. 2015;20(1):37-46. IF: 2.583.

33. Teleki I, Szasz AM, **Maros ME**, Gyorffy B, Kulka J, Meggyeshazi N, Kiszner G, Balla P, Samu A, Krenacs T. Correlations of differentially expressed gap junction connexins Cx26, Cx30, Cx32, Cx43 and Cx46 with breast cancer progression and prognosis. PLoS One. 2014;9(11):e112541. IF: 3.234.

34. Kiszner G, Wichmann B, Nemeth IB, Varga E, Meggyeshazi N, Teleki I, Balla P, **Maros ME**, Penksza K, Krenacs T. Cell cycle analysis can differentiate thin melanomas from dysplastic nevi and reveals accelerated replication in thick melanomas. Virchows Arch. 2014;464(5):603-12. IF: 2.651.

Impact factors as first- or last author not directly related to the dissertation: 57.172.
Impact factors as coauthor not directly related to the dissertation: 78.098.
Sum of impact factors not directly related to the dissertation: 135.27.

10. Acknowledgements

I am extremely grateful to Professor András Matolcsy for inviting me to undertake my Scientific Students' Associations (TDK) project at the department and later for letting me pursue my doctoral journey at the institution. I am thankful to the Doctoral Committee for allowing me to carry out my research as an individual graduate in the Doctoral School of Pathological Sciences.

I would like to express my deepest gratitude to my supervisor Professor Tibor Krenács for his trust in giving me the opportunity to join his lab and for his tremendous support and understanding over the years. For allowing me to carry out my doctoral thesis as a clinician despite the challenges. I am tremendously thankful for his patience and paternal guidance along the way. I am especially grateful for him being my most important research tie to home. I could not have asked for more.

Special thanks to each member of our lab: Dres. Péter Balla, Ivett Teleki, Gergő Kiszner, Nóra Meggyesházi and Edit Parsch† for making the time fly by in the lab and for becoming trusted friends for life. Also, Éva Mátrai Balogh for her technical assistance. Thanks to my dear friend dr. Zoltán Kelemen for our endless TMA scoring sessions.

I would like to thank: Professor László Kopper, Professor Miklós Szendrői and Professor Zoltán Sápi for laying down the cornerstones of the EuroBoNet research program that provided the opportunity to pursue this research project. I am greatly indebted to Professor Piero Picci and Dr. Maria Serena Benassi from the Institute of Rizzoli Bologna for providing the specimens and clinical data.

Many thanks to my dear friend Professor Holger Wenz for his support during tough times and for reminding me to keep my eyes on the target. Thanks should also go to Professor Christoph Groden, head of the Dept. of Neuroradiology, Medical Faculty Mannheim, Heidelberg University to consent to me embarking on this journey. Also, thanks to Dr. Sven Schnaidt for his statistical support.

Finally, I would like to thank my beloved Mother from the bottom of my heart for her unconditional love, support, endurance and tolerance. She made everything I have accomplished in life possible!